POLITECNICO DI TORINO

Facoltà di Ingegneria
Corso di Laurea in Ingegneria Aerospaziale

Tesi di Laurea Magistrale

Escape maneuvers with lunar gravity assists

Relatore:
prof. Lorenzo Casalino

Candidato:
Alex Siniscalco

Anno accademico 2017-2018

'Nothing is achieved without
sacrifice and courage ...
Who is capable to suffer
will eventually win'

Mahatma Gandhi

Abstract

For spacecraft interplanetary missions, gravity assist maneuvers are usually used because they allow one to get as a rule high ΔV without having to use propellant, but exploiting the energy given by the gravitational attraction of a celestial body. This allows improving the useful mass for a specific mission, for a modest increase in flight time. Thus, when escape from Earth's sphere of influence is regarded, lunar gravity assist maneuvers become a valid alternative to direct escapes.

In this paper, two consecutive gravity assist maneuvers are considered and the possible moon-to-moon trajectories that allow them are sought. Afterwards, considering different spacecraft initial velocities relative to Moon, the effect on the escape orbit is analyzed, with the purpose to link the features of the latter (i.e the heliocentric flight-path angle and declination) to the maximum obtainable specific mechanical energy (i.e. the achievable escape velocity).

First, a brief introduction will be presented, followed by a chapter dedicated to the mathematical models adopted to carry out the thesis; after that, will be illustrated the technique used for the study of moon-to-moon orbits and lunar gravity assists, followed by a description of the attained results. Finally, the conclusive observations, in addition to the problems faced during the analysis and a short debate on the possible future developments of the present work, will be introduced in a dedicated chapter.

Contents

List of Tables

List of Figures

Chapter 1

Introduction

In order to develop an interplanetary mission there are two important aspects to consider: the definition of the escape trajectory, which allows to the spacecraft to go out of the Earth's sphere of influence (i.e. the spheroidal region of space where the Earth gravitational pull prevails) and the associated maneuver, which allows to the spacecraft to reach the wanted heliocentric orbit. The choice of escape strategy used is important, since it affects the cost of the mission in reference to propellant necessary that directly influence the payload mass that can be carried. There are different escape strategies for a specific mission, those usually used are:

- direct escape – a single-impulse maneuver leading the spacecraft on an hyperbolic orbit, that after is travelled until when the escape conditions are not reached, i.e. the wanted hyperbolic excess velocity; this strategy needs of a high-thrust propulsion system, that uses chemical propellants;

- Oberth maneuver (powered flyby) - two single-impulse maneuvers are used that allow reducing the gravitational losses: the first allows decreasing the spacecraft's velocity while to move closer to the main body with an Hohmann transfer and the second, given to the periastron now lowered, bringing the spacecraft on an hyperbolic escape orbit, analogous to the one of the direct escape. The gravitational losses are

minimized because the second impulse is provided at higher velocity (i.e to lower altitude). With this escape maneuver is obtained an inferior global ΔV, but it is possible only when the chemical propulsion is utilized. However, starting from a LEO orbit this maneuver is not feasible, as it would lead to a collision;

- low-thrust escape – a continuous thrust is used, lightly directed to the main body, bringing the spacecraft on a spiral orbit. This escape maneuver allows reducing gravitational losses accepting an increased of misalignment losses. It is used when the spacecraft has an electric propulsion system, which allows obtaining low acceleration values, usually in the range of 1 mm/s^2, but higher specific impulse respect to chemical propulsion. However, the disadvantage is due to its duration, that can be several years;

- gravity assist – the exchange of momentum between the spacecraft and the celestial body chosen is used to rotate the spacecraft's relative velocity to obtain a ΔV, without consumption of specific propellant, both chemical or electrical. Since much convenient, it is sometimes used to non-escape trajectories, over that for escape ones, which is the principal argument of this paper.

The gravity assist maneuvers, especially the lunar ones, are commonly used to mission towards asteroids. A particular example is Asteroid Redirect Robotic Mission (ARRM), which is designed to characterize a 100+ m class near-Earth asteroid and to capture and recover a 1-6 m maximum extent boulder off of the surface of the asteroid and bring it into cislunar space.
The Asteroid Redirect Vehicle (ARV) is launched on either a Delta IV Heavy or Falcon Heavy launch vehicle to a trajectory directed towards the moon, where is then carried out two lunar gravity assist (LGA): the first sends the ARV onto a large, distant Earth orbit where solar perturbations increase its energy before of the second LGA that sends it onto an Earth escape trajectory. During this phase non-critical deployments and checkouts are conducted, where the Solar Electric Propulsion system is calibrated and pre-

pared for interplanetary thrust. When the ARV reach the asteroid, the said above operations are carried out on it. After, an inbound cruise then takes the combined ARV and boulder back to Earth, where before another LGA is performed that sends ARV-boulder combination into the Earth-Moon system and they are then transferred to a crew-accessible orbit, using solar and lunar perturbations. Finally, a crew on the other spacecraft, rendezvous and dock the ARV, which is transferred to a Lunar Distant Retrograde Orbit (DRO) with an orbit lifetime in excess of 100 years for storage of the returned boulder.

The goal of the present study is to analyze the possibility of using the energy obtained by multiple lunar gravity assist maneuvers to escape from earth's gravitational attraction and reach asteroids. Particularly, two consecutive gravity assist maneuvers have been considered and the possible moon-to-moon trajectories that allow them have been searched.
In the chapter 2 of this thesis will be discussed the mathematical models will be used for the analysis: the general N-body problem, which will be then extended to the problem of two and three bodies, that will allow defining the coplanar moon-to-moon trajectory among the two gravity assist maneuvers, followed by an example of a lunar gravity maneuvre, to understand the rationale.
In the chapter 3 will be presented the designed codes for both the gravity assist trajectory and the evaluation of the escape conditions according to the wanted heliocentric flight-path angle and declination of the spacecraft velocity vector.
The obtained results will be presented in chapter 4, where, for different spacecraft initial velocitys relative to Moon, the found moon-to-moon transfers will be shown, jointly with the graphs that correlate flight-path angle and declination to the characteristic energy and escape velocity.
Finally, in chapter 5 will be exposed the conclusive observations, over to the problems faced during the analysis and a short discussion about possible future developments.

Chapter 2

Mathematical model

In this chapter will focus on the circular restricted three body problem that has been adopted to define the desired trajectories. At the beginning, the general N-body problem will be analyzed, which will be then extended to the problem of two and three bodies, with a little bracket on the constants of motion. Finally, after a discussion on the patched-conic approximation, the mathematical model used for the study of the gravity assist maneuver will be presented.

2.1 The N-body problem

The N-body problem model explains the mutual gravitational interaction between N masses in such a way to determine their motion. This can be done using Newton's law of universal gravitation, introduced in his *Philosophiæ Naturalis Principia Mathematica* in 1686 [8].

Newton's law of universal gravitation
Any two bodies attract one another with a force along their joining line which is proportional to the product of their masses and inversely proportional to the square of their distance.

This law can be written mathematically in vector notation[1]:

$$\boldsymbol{F_g} = -G\frac{mM}{r^2}\frac{\boldsymbol{r}}{r} \tag{2.1}$$

This equation expresses the force $\boldsymbol{F_g}$ that the body of mass M applies onto the body of mass m, where $\boldsymbol{r}$ is the position vector of m respect to M and G is the universal gravitational constant, whose value is $G = 6.67259 \cdot 10^{-11} m^3/(kg \cdot s^2)$. It is noted that there is a negative sign at the second member which underline the attractive nature of the gravitational force.
To understand another concept, Newton's third law is called back:

Newton's third law
Every force exerted on object B by another object A, object B will instantly exert another force with same magnitude but opposite direction on object A.

In addition to the force on m applied by M there is another force on M generated by m, which has same intensity, but opposite direction.

An inertial reference system (X, Y, Z) is considered, where a system consisting of n masses $(m_1, m_2 \dots m_i \dots m_n)$ will be placed, the coordinates of which are individuated by position vectors $(\boldsymbol{r_1}, \boldsymbol{r_2} \dots \boldsymbol{r_i} \dots \boldsymbol{r_n})$, as shown in figure 2.1. Before Newton's second law are used to determine the motion of the i^{th} body, the combined force acting on m_i is identified.

Newton's second law
The rate of change of momentum of an object is proportional to the force impressed on it and is the same direction as that force.

The mathematical expression of such law is the followed:

$$\sum \boldsymbol{F} = \frac{d}{dt}\left(m_i \dot{\boldsymbol{r}}_{\boldsymbol{i}}\right) \tag{2.2}$$

[1]In this paper will be used the convention for which vectors are represented by bold font while scalars with regular font.

The resultant force acting on m_i can be written as:

$$\sum \boldsymbol{F} = \boldsymbol{F_g} + \boldsymbol{F_{other}}$$

Here $\boldsymbol{F_g}$ groups the gravitational effects of each mass in the system except mi, whereas $\boldsymbol{F_{other}}$ encloses all other kinds of forces (such as thrust, perturbations, atmospheric drag or solar pressure). Therefore, the global effect of gravitational forces $\boldsymbol{F_g}$ can be expressed using equation 2.1, where $\boldsymbol{r_{ji}}$ is the vector linking the j^{th} and the i^{th} masses.

$$\boldsymbol{F_g} = -Gm_i \sum_{\substack{j=1 \\ j \neq i}}^{n} \frac{m_j}{{r_{ji}}^3} \boldsymbol{r_{ji}} \tag{2.3}$$

Finally, expanding equation 2.2, the equation describing the motion of the i^{th} body is obtained:

$$\boldsymbol{\ddot{r}_i} = -G \sum_{\substack{j=1 \\ j \neq i}}^{n} \frac{m_j}{{r_{ji}}^3} \boldsymbol{r_{ji}} + \frac{\boldsymbol{F_{other}}}{m_i} - \boldsymbol{\dot{r}_i} \frac{\dot{m}_i}{m_i} \tag{2.4}$$

The resolution of the N-body problem presented above is substantially complexity, therefore simplifying hypotheses are introduced, that do not compromise the reliability of the results, but they make the problem no longer completely descriptive of the real phenomenon. The hypotheses are:

- the involved bodies are uniform and spherical, in order to consider them punctiform;
- the involved bodies are constant in time (this second assumption is often rather accurate, e.g. when talking about a satellite on a Newtonian orbit, i.e. with thrusters off);
- all kind of external perturbation are ignored and only the gravitational force is considered.

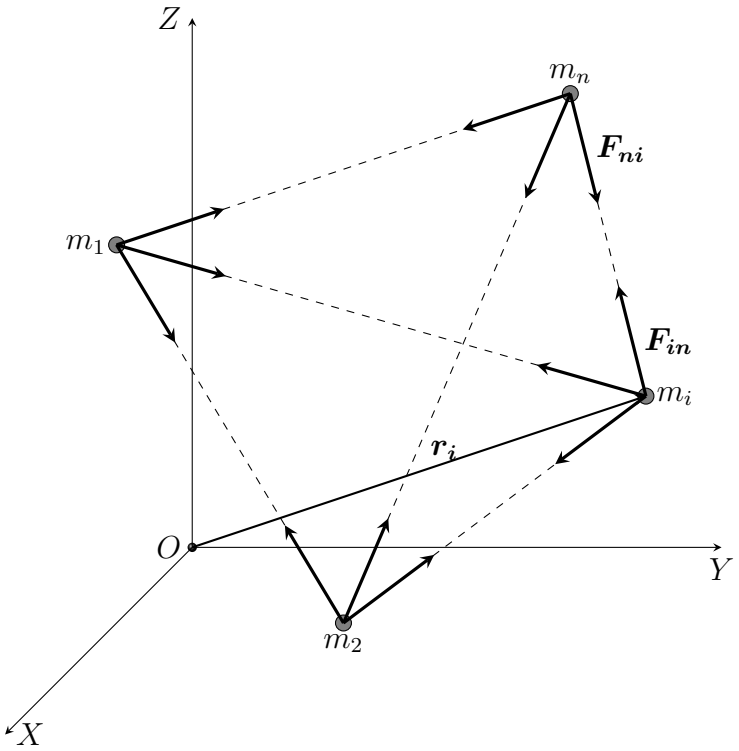

Figure 2.1: The N-body problem.

Consequently, $\boldsymbol{F_{other}}$ and $\dot{m}_i$ are null and the equation 2.4 can be written as followed:

$$\ddot{\boldsymbol{r}}_{\boldsymbol{i}} = -G \sum_{\substack{j=1 \\ j \neq i}}^{n} \frac{m_j}{{r_{ji}}^3} \boldsymbol{r_{ji}} \tag{2.5}$$

Now, it is necessary to rewrite this equation, because the aim is usually to express the motion of the i^{th} body respect to another body (e.g the motion of Earth orbiting the sun), whereas it expresses the motion respect to the inertial reference frame.

For instance, to express the motion of m_2 relatively to m_1, the equations of motion in the inertial reference system of both bodies need to be written:

$$\begin{cases} \ddot{\boldsymbol{r}}_{\boldsymbol{1}} = -G \sum_{j=2}^{n} \frac{m_j}{{r_{j1}}^3} \boldsymbol{r_{j1}} \\ \ddot{\boldsymbol{r}}_{\boldsymbol{2}} = -G \sum_{\substack{j=1 \\ j \neq 2}}^{n} \frac{m_j}{{r_{j2}}^3} \boldsymbol{r_{j2}} \end{cases} \tag{2.6}$$

After, using the 2.1, the position of body 2 in relation to body 1 can be expressed:

$$\boldsymbol{r_{12}} = \boldsymbol{r_2} - \boldsymbol{r_1} \tag{2.7}$$

Equally, a similar equation is written for accelerations:

$$\ddot{\boldsymbol{r}}_{\boldsymbol{12}} = \ddot{\boldsymbol{r}}_{\boldsymbol{2}} - \ddot{\boldsymbol{r}}_{\boldsymbol{1}} \tag{2.8}$$

Therefore, the motion's equation of the secondary body around the main one can be obtained subtracting equation for mass m_1 from the other:

$$\ddot{\boldsymbol{r}}_{\boldsymbol{12}} = -G \sum_{\substack{j=1 \\ j \neq 2}}^{n} \frac{m_j}{{r_{j2}}^3} \boldsymbol{r_{j2}} + G \sum_{j=2}^{n} \frac{m_j}{{r_{j1}}^3} \boldsymbol{r_{j1}} \tag{2.9}$$

Collecting the proportional terms to $\boldsymbol{r_{12}}$ and underlining how $\boldsymbol{r_{21}} = -\boldsymbol{r_{12}}$, equation 2.9 can be rewritten as:

$$\ddot{\boldsymbol{r_{12}}} = -G\frac{m_1 + m_2}{{r_{12}}^3}\boldsymbol{r_{12}} - G\sum_{j=3}^{n} m_j \left(\frac{\boldsymbol{r_{j2}}}{{r_{j2}}^3} - \frac{\boldsymbol{r_{j1}}}{{r_{j1}}^3}\right) \tag{2.10}$$

2.2 The 2-body problem

Although the simplifying hypotheses have been introduced, the solution to the N-body problem remains anyway complex, since equation 2.10 is a second order, non-linear, vector, differential equation of motion, which requires numerical integration to find a solution. Nevertheless, it is possible to search an analytic solution to such problem by reducing the number of bodies involved to two: a main body M and a secondary one m orbiting the first. Another hypothesis is introduced:

- the mass of the secondary body is notably inferior to that of the primary one ($m \ll M$).

An inertial reference system (X', Y', Z') and a non-rotating reference system parallel to the previous one (X, Y, Z) are taken, whose origin coincides with the position of the main body. Moreover, as shown in figure 2.2, with $\boldsymbol{r_M}$ and $\boldsymbol{r_m}$ the position vectors of the two bodies in the inertial system and with $\boldsymbol{r}$ the position vector of m in (X, Y, Z) are indicated.
Equation 2.10 can then be rewritten as:

$$\ddot{\boldsymbol{r}} = -G\frac{m + M}{r^3}\boldsymbol{r} \tag{2.11}$$

Using the hypothesis introduced previously ($m \ll M$), $m + M \simeq M$. Introducing also the gravitational parameter $\mu = GM$, the following equation is obtained:

$$\ddot{\boldsymbol{r}} = -\frac{\mu}{r^3}\boldsymbol{r} \tag{2.12}$$

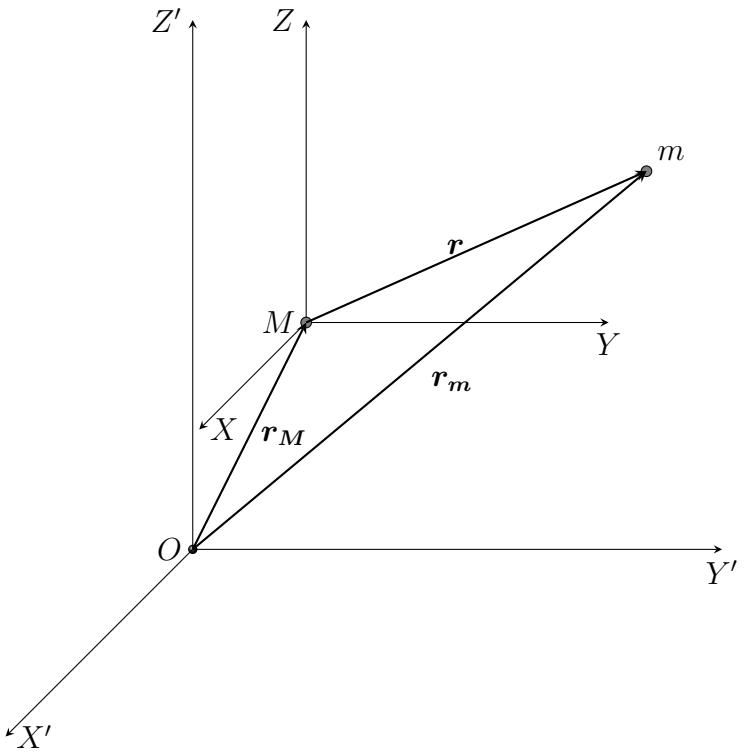

Figure 2.2: Relative motion of 2 bodies.

2.3 Constants of the motion

Before to integrate the equation of motion to obtain the equation of the trajectory, it is necessary to define some constants that characterize orbital motion itself: the specific angular momentum (h) and specific mechanical energy ($\mathscr{E}$).

2.3.1 Specific angular momentum

The angular momentum of an orbiting body keeps its magnitude and direction when no force other than the gravitational one acts on the system.
This can be demonstrated by going initially to multiply both terms of equation 2.12 to the left by $\boldsymbol{r}$:

$$\boldsymbol{r} \times \ddot{\boldsymbol{r}} = -\boldsymbol{r} \times \frac{\mu}{r^3}\boldsymbol{r} \tag{2.13}$$

Since a vector is always parallel to itself, the vector product $\boldsymbol{r} \times \boldsymbol{r} = 0$, thus the second member disappears:

$$\boldsymbol{r} \times \ddot{\boldsymbol{r}} = 0 \tag{2.14}$$

It is to be highlighted, however, that:

$$\frac{d}{dt}(\boldsymbol{r} \times \dot{\boldsymbol{r}}) = \boldsymbol{r} \times \ddot{\boldsymbol{r}} + \dot{\boldsymbol{r}} \times \dot{\boldsymbol{r}} \tag{2.15}$$

Also here $\dot{\boldsymbol{r}} \times \dot{\boldsymbol{r}} = 0$ for the same reason indicated above, thus it can be deduced that $\boldsymbol{r} \times \dot{\boldsymbol{r}} = const.$ since its derivative is null. As $\dot{\boldsymbol{r}} = \boldsymbol{V}$ is the velocity vector, it is obtained that the vector product $\boldsymbol{r} \times \boldsymbol{V}$ is a constant of motion, called specific angular momentum ($\boldsymbol{h}$).
How much just demonstrated, i.e that h is constant, brings to an important conclusion: being the angular momentum the cross product of $\boldsymbol{r}$ and $\boldsymbol{V}$, it is a vector perpendicular to both; but, since it is constant in magnitude and direction, $\boldsymbol{r}$ and $\boldsymbol{V}$ will always stay on the same plane. Thus, Newtonian orbits are confined to a plane, which we shall call orbital plane.

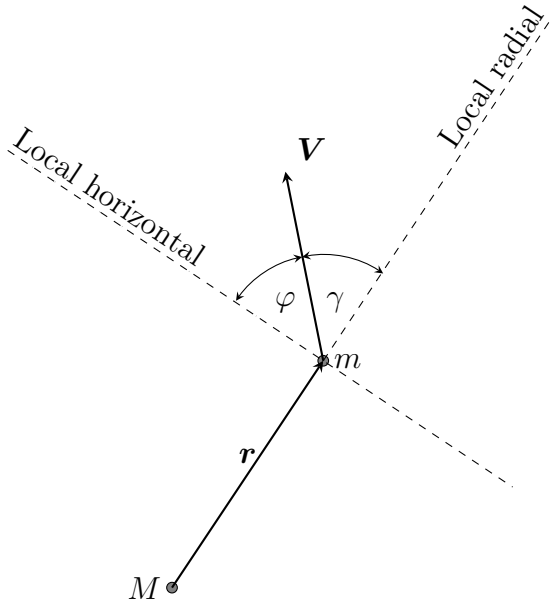

Figure 2.3: Zenit and flight-path angle.

Finally, using the flight-path angle φ (i.e. the angle between the velocity vector and the local radial), which is complementary to the zenith angle (γ), as shown in figure 2.3, the magnitude of $\boldsymbol{h}$ can be linked with the direction of $\boldsymbol{V}$, through the following expression:

$$h = rV\cos\varphi \tag{2.16}$$

2.3.2 Specific mechanical energy

Another constant of motion characterizing every orbit is the specific mechanical energy $\mathscr{E}$, i.e. the sum of potential and kinetic energy per unit mass.
In order to demonstrate this, initially, the equation 2.12 is dot multiplied by $\dot{\boldsymbol{r}}$:

$$\dot{\boldsymbol{r}} \cdot \ddot{\boldsymbol{r}} + \dot{\boldsymbol{r}} \cdot \frac{\mu}{r^3}\boldsymbol{r} = 0 \tag{2.17}$$

That can be rewritten as:

$$\dot{r}\ddot{r} + \dot{r}\frac{\mu}{r^2} = 0 \tag{2.18}$$

It can be observed that $\dot{r} = V$ and that:

$$\begin{cases} V\dot{V} = \dfrac{d}{dt}\left(\dfrac{V^2}{2}\right) \\ \dot{r}\dfrac{\mu}{r^2} = \dfrac{d}{dt}\left(-\dfrac{\mu}{r}\right) \end{cases} \tag{2.19}$$

Therefore, it is possible to write:

$$\frac{d}{dt}\left(\frac{V^2}{2} - \frac{\mu}{r}\right) = 0 \tag{2.20}$$

Getting so the want equation:

$$\mathscr{E} = \frac{V^2}{2} - \frac{\mu}{r} + C = const. \tag{2.21}$$

In this equation there are three terms:

- $\dfrac{V^2}{2}$ is the kinetic energy per unit mass, which expresses the energy contribution due to motion;
- $-\dfrac{\mu}{r}$ is the potential energy per unit mass due to the gravitational field, depending only on the position of the orbiting body and the mass of the main body;
- C is a constant term coming from the integration of equation 2.20 and being its value arbitrary, it can be then set equal to zero (this is equivalent to choosing the zero reference for potential energy at infinity).

2.4 Equation of the trajectory

After having defined the constants that characterize orbital motion, it is now possible to integrate twice equation 2.12 in order to get the trajectory equation for the 2-body problem. However, instead of proceeding to the integration of the equation as it is, it is manipulated to find derivatives.
It is first multiplied by the specific angular momentum vector ($\boldsymbol{h}$):

$$\ddot{\boldsymbol{r}} \times \boldsymbol{h} = \frac{\mu}{r^3} (\boldsymbol{h} \times \boldsymbol{r}) \tag{2.22}$$

In the left term of equation 2.22 can be recognized immediately a derivative, since:

$$\frac{d}{dt} (\dot{\boldsymbol{r}} \times \boldsymbol{h}) = (\ddot{\boldsymbol{r}} \times \boldsymbol{h}) + (\dot{\boldsymbol{r}} \times \cancelto{0}{\dot{\boldsymbol{h}}}) \tag{2.23}$$

Instead, the right term can be transformed into the time rate of change of another vector quantity:

$$\begin{aligned} \frac{\mu}{r^3} (\boldsymbol{h} \times \boldsymbol{r}) &= \frac{\mu}{r^3} (\boldsymbol{r} \times \boldsymbol{V}) \times \boldsymbol{r} = \\ &= \frac{\mu}{r^3} [\boldsymbol{V} (\boldsymbol{r} \cdot \boldsymbol{r}) - \boldsymbol{r} (\boldsymbol{r} \cdot \boldsymbol{V})] = \\ &= \frac{\mu}{r} \boldsymbol{V} - \frac{\mu \dot{r}}{r^2} \boldsymbol{r} = \\ &= \mu \frac{d}{dt} \left(\frac{\boldsymbol{r}}{r} \right) \end{aligned} \tag{2.24}$$

The equation 2.12 become the following:

$$\frac{d}{dt} (\dot{\boldsymbol{r}} \times \boldsymbol{h}) = \mu \frac{d}{dt} \left(\frac{\boldsymbol{r}}{r} \right) \tag{2.25}$$

Integrating the equation 2.25, it is obtained:

$$\dot{\boldsymbol{r}} \times \boldsymbol{h} = \mu \frac{\boldsymbol{r}}{r} + \boldsymbol{B} \tag{2.26}$$

In this equation $\boldsymbol{B}$ represent a vector constant produced by the integration process.
Then the equation 2.26 is dot multiplied by $\boldsymbol{r}$:

$$\boldsymbol{r} \cdot \dot{\boldsymbol{r}} \times \boldsymbol{h} = \mu \frac{\boldsymbol{r} \cdot \boldsymbol{r}}{r} + \boldsymbol{r} \cdot \boldsymbol{B} \tag{2.27}$$

The equation just obtained, denoting with ν the angle between $\boldsymbol{B}$ and $\boldsymbol{r}$ and using the vector identities, can be rewritten in the following way:

$$h^2 = \mu r + rB \cos \nu \tag{2.28}$$

Solving for r, the trajectory equation is achieved:

$$r = \frac{\dfrac{h^2}{\mu}}{1 + \dfrac{B}{\mu} \cos \nu} \tag{2.29}$$

This equation is equal to the equation of a conic section expresses in polar coordinates with origin in one of the foci.

$$r = \frac{p}{1 + e \cos \nu} \tag{2.30}$$

Where p is the semilatus rectum and e the eccentricity, while ν, as in equation 2.29, is the angle included between the point of the conic closest to the focus (called periastron) and $\boldsymbol{r}$.

2.5 The circular restricted 3-body problem

The 2-body model, previously described, does not describe accurately the orbital motion of the spacecraft between the two maneuvers of lunar gravity assist, since it does not consider the remarkable role done by the sun. Therefore, the circular restricted 3-body model is adopted, which includes also the sun together Earth and the spacecraft. However, using this model can't be found an analytical solution, but to simplify it, also in this case, can be made some assumption, without sacrificing accuracy.

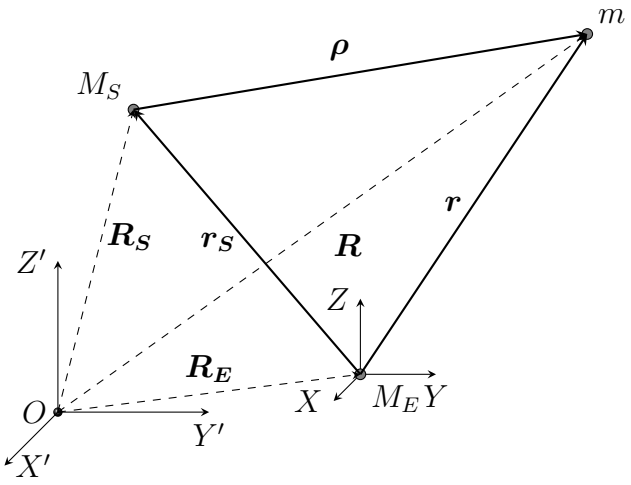

Figure 2.4: The 3-body problem in an inertial reference.

The assumptions are:

- during the calculations, only two of three masses considered are used (i.e. the spacecraft's mass is negligible);
- the main bodies (m_S and m_E) move on a circular orbit around their shared centre of mass.

Consider the Earth-Sun-spacecraft system, as shown in figure 2.4.

In order to obtain the vector equation describing the motion of the spacecraft respect to Earth, first of all the gravitational effect of the three bodies needs to be written mathematically in the inertial reference system, using equation 2.1:

$$\begin{cases} m\ddot{\boldsymbol{R}} = -G\dfrac{mM_E}{r^2}\dfrac{\boldsymbol{r}}{r} - G\dfrac{mM_S}{\rho^2}\dfrac{\boldsymbol{\rho}}{\rho} & \text{for the spacecraft} \\ M_E\ddot{\boldsymbol{R}}_{\boldsymbol{E}} = G\dfrac{M_E m}{r^2}\dfrac{\boldsymbol{r}}{r} + G\dfrac{M_E M_S}{r_S^2}\dfrac{\boldsymbol{r_S}}{r_S} & \text{for Earth} \\ M_S\ddot{\boldsymbol{R}}_{\boldsymbol{S}} = -G\dfrac{M_S M_E}{r_S^2}\dfrac{\boldsymbol{r_S}}{r_S} + G\dfrac{M_S m}{\rho^2}\dfrac{\boldsymbol{\rho}}{\rho} & \text{for the Sun} \end{cases} \tag{2.31}$$

Thus, subtracting the Earth's equation from one for the spacecraft, considering that $\boldsymbol{r} = \boldsymbol{R} - \boldsymbol{R_E}$ and using the hypothesis previously enunciated ($m \ll M_E, M_S$), the equation of motion of the spacecraft respect to Earth is obtained:

$$\ddot{\boldsymbol{r}} = -G\frac{M_E}{r^3}\boldsymbol{r} - GM_S\left(\frac{\boldsymbol{\rho}}{\rho^3} + \frac{\boldsymbol{r_S}}{r_S^3}\right) \tag{2.32}$$

Turning this equation into a system of six first-order differential equations, the trajectory solution is found by numerical integration.

2.6 Gravity assist

For spacecraft interplanetary missions, gravity assist maneuvers are usually used because they allow one to get generally high ΔV without having to use propellant, but exploiting the energy provided by the gravitational attraction of a celestial body. Rotating the spacecraft's relative velocity of the body itself can be obtained a positive or negative ΔV; due to this rotation, both in direction and magnitude, the absolute velocity in the inertial reference system is modified, because it can be obtained as the vector sum of the velocity of the mass around which the maneuver takes place and the spacecraft's relative velocity.

This chapter is first focused on the patched-conic approximation and after an example of a lunar gravity assist maneuver is discussed, to understand the rationale.

2.6.1 The patched-conic approximation

When interplanetary missions are carried out, it is necessary to take into account that a spacecraft is principally subject to the gravitational influence of the sun, while perturbations due to other celestial bodies interfere on its motion only when it itself is in their proximity. Therefore, the motion of spacecraft can be approximated by dividing it into different conic orbits

around each mass the gravitational attraction of which is not neglected, and patching them together at the edge of the spheres of influence (i.e. a spherical portions of space within which the gravitation pull of a single body predominate). For a preliminary analysis of a space mission, this approximation allow obtaining results quite accurate, although it does not give a realistic description of the phenomenon, since the transition from orbiting a body to another is a gradual process and does not happen instantaneously.
In this paper the definition of the sphere of influence presented by Laplace is used; for example, the sphere of influence of Earth's gravitational field on the moon is centered at the moon and has radius:

$$r_s = R_{E-M} \left(\frac{M_M}{M_E} \right)^{\frac{2}{5}} \tag{2.33}$$

This equation depends on the two bodies considered, especially their distance and their masses.

The patched-conic approximation results much useful when maneuvers in close of a celestial body are analyzed. For instance, during a preliminary analysis of lunar gravity assists, only the moon's sphere of influence can be considered and all other gravitational effects and perturbations can be neglected.

2.6.2 Lunar gravity assist

It is examined a lunar gravity assist maneuver carried out by spacecraft headed to it. As shown in figure 2.5, considering a planar case for simplicity, when the spacecraft arrives in the moon's sphere of influence, the 2-body model can be used to represent the problem, where the moon is the main body and the spacecraft is the orbiting one.

It can be observed that in the Earth-centered reference the spacecraft reaches the moon sphere of influence with a velocity $\boldsymbol{V}_{\boldsymbol{S/C}}^{-}$. However, since it is desired to describe the motion with the 2-body model, it is necessary to express the

spacecraft's velocity respect to the moon:

$$\boldsymbol{V_\infty^-} = \boldsymbol{V_{S/C}^-} - \boldsymbol{V_M} \tag{2.34}$$

The angle between $\boldsymbol{V_M}$ and $\boldsymbol{V_\infty^-}$ is the pump angle before LGA (p^-), which is important to evaluate the effectiveness of the maneuver.
Known V_∞^-, it can be drawn the spacecraft's orbit, which is a hyperbola, since to enter in the sphere of influence V_∞^- must be greater than 0 and its edge can be approximated by $r \to \infty$. The spacecraft treads along the orbit and escapes the sphere of influence with a relative velocity V_∞^+, which is equal to V_∞^- due to the conservation of mechanical energy:

$$\mathscr{E} = \frac{V_\infty^{-2}}{2} - \cancelto{0}{\frac{\mu}{r}} = \frac{V_\infty^{+2}}{2} - \cancelto{0}{\frac{\mu}{r}} \tag{2.35}$$

It is observed that the direction of $\boldsymbol{V_\infty}$ is modified by an angle $\delta = \pi - 2\phi$, where $\phi = \arccos(1/e)$ is the opening angle of the hyperbola of eccentricity e, while its magnitude remains constant. Therefore, also the angle $\boldsymbol{V_\infty}$ forms with $\boldsymbol{V_M}$ is changed ($p^- \neq p^+$), thus:

$$\boldsymbol{V_{S/C}^+} = \boldsymbol{V_M} + \boldsymbol{V_\infty^+} \neq \boldsymbol{V_{S/C}^-} \tag{2.36}$$

The gravity assist maneuver allows then obtaining a ΔV – to accelerate or decelerate a spacecraft – without consumption of propellant. This is possible thank to the conservation of angular momentum for the moon-spacecraft system. Indicating with $\boldsymbol{r_s}$ the radius of the lunar sphere of influence, it is had:

$$\Delta H = m r_s \Delta V - M_M r_s \Delta V_M = 0 \tag{2.37}$$

Therefore, simplifying r_s:

$$\Delta V_M = \frac{m}{M_M} \Delta V \tag{2.38}$$

Since the spacecraft's mass is much smaller than the mass of the moon ($m \ll M_M$), the effect on the moon's velocity is negligible.

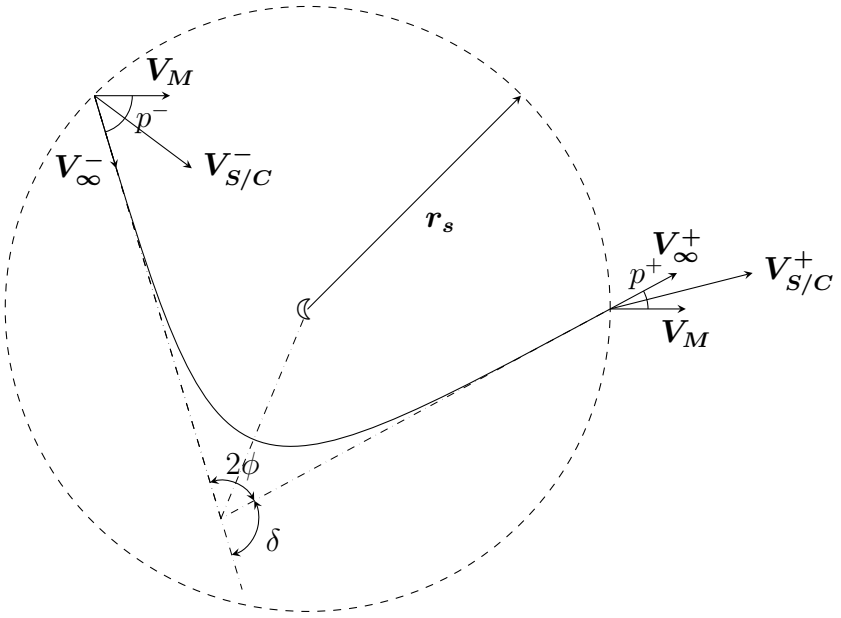

Figure 2.5: Geometrical schema for a generic lunar gravity assist manoeuvre.

However, gravity assists influence also the inclination of the orbit, producing a Δi and a ΔV. Therefore, in general, over the pump angle, it is then necessary to introduce the crank angle to accurately identify the three components of the velocity vector: radial, tangential, and normal (figure 2.6).

$$\begin{cases} u_\infty = V_\infty \sin p \cos k \\ v_\infty = V_\infty \cos p \\ w_\infty = V_\infty \sin p \sin k \end{cases} \tag{2.39}$$

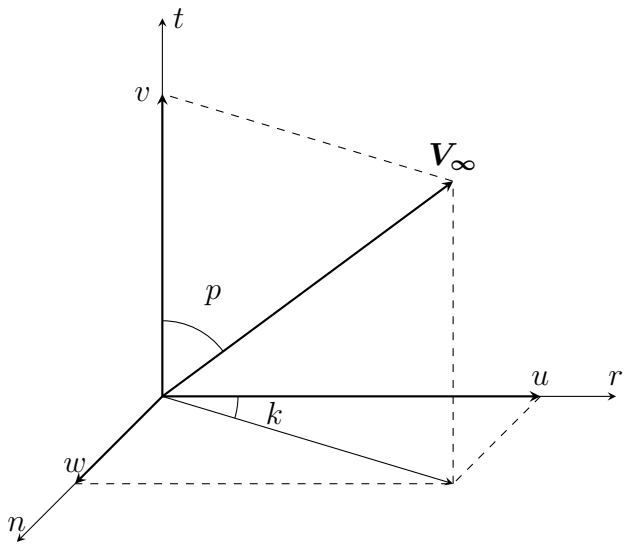

Figure 2.6: Components of $\boldsymbol{V}_\infty$ expressed via pump (p) and crank (k) angles.

Chapter 3

Analysis

3.1 Solar-perturbed moon-to-moon transfer

The analysis of the moon-to-moon transfer between the two gravity-assist maneuvers is performed using the circular restricted 3-body model, which takes into account the perturbative effect of the sun on the spacecraft's motion. Moreover, a planar hypothesis has been used: each body involved lies on the same plane $X - Y$ and each vector does not have a Z component.

Another simplification, considering a non-rotating reference system centered on Earth, is to fix the transfer starting point at the intersection between the moon orbit and the x axis ($\theta_{M_0} = 0°$), as to make easier the comparison among the various orbits and underline their differences. Besides, two different orbits categories can be distinguished :

- outbound-inbound - outbound-inbound - initially the spacecraft moves away from Earth and then it gets closer to it;
- inbound-inbound - initially the spacecraft moves closer to Earth, then it moves away from it and successively it gets closer to it again.

In order to study the effect of the magnitude of the spacecraft's velocity vector relative to the moon on the orbits, the following different velocities are used: $V_\infty = 0.9\ km/s$, $V_\infty = 1\ km/s$ and $V_\infty = 1.1\ km/s$. From this last one

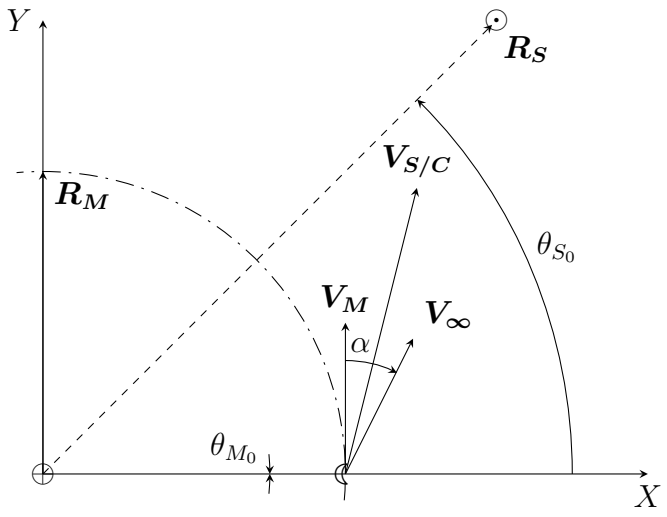

Figure 3.1: Geometrical schema for determination of moon-to-moon transfer orbits. Here the outbound-inbound example is shown, being $\alpha > 0$.

a velocity relative to the inertial reference is obtained $\boldsymbol{V_{S/C}} = \boldsymbol{V_M} + \boldsymbol{V_\infty}$, where $\boldsymbol{V_M}$ is the moon velocity vector relative to Earth.
The first variable parameter is the angle α between $\boldsymbol{V_\infty}$ and $\boldsymbol{V_M}$, which define the inner loop of the iteration process – varying from 0° to 180° for the outbound-inbound orbits and from −0.05° to −179.95° for the inbound-inbound, in 0.05° steps. The initial position of the sun (θ_{S_0}) is the second varying parameter, which cycles from 0° to 359° in 1° increments, determining the outer loop. In figure 3.1 is presented a sketch of the geometry of the issue.

Using the following initial conditions, the designed program integrates the equations of motion (2.32).

$$\begin{cases} X_0 = R_M \cos(\theta_{M_0}) \\ Y_0 = R_M \sin(\theta_{M_0}) \\ Z_0 = 0 \\ V_{X_0} = -V_M \sin(\theta_{M_0}) - V_\infty \sin(\theta_{M_0} - \alpha) \\ V_{Y_0} = V_M \cos(\theta_{M_0}) + V_\infty \cos(\theta_{M_0} - \alpha) \\ V_{Z_0} = 0 \end{cases} \tag{3.1}$$

To avoid unreasonable flight times, an integration period of 7 months has been chosen, but if an encounter with the lunar orbit is found, the integration is stopped earlier and the moon's and spacecraft's angular positions are then compared with those obtained in the previous iteration; if there is an inversion of sign, a subroutine is called, which identify the exact value of α that allows a spacecraft-moon re-encounter, reaching convergence with the secant method.

The procedure described might not converge and miss some solutions, thus, to use it, a systematic search of solutions with sun's initial position translated by $\pm 180°$ is inserted, which take into account that the sun gravitational perturbation has an almost exact 180° periodicity with respect to the latter.

$$\theta_{S_0,sym} = \theta_{S_0} + \pi \tag{3.2}$$

As the deviations have the same order of magnitude of $\frac{r}{r_S}$, available moon-to-moon trajectories are expected to show same periodicity.
Moreover, the search for α_{sym} that are associated to a correct solution is limited to the range α, due to the just mentioned symmetry.

Another aspect to underline is many of the found solutions are not significative in the context of this analysis: several duplicates and solutions, which do not have a physical meaning are identified. The first have the unsought effect of slowing down computation and leading no advantage, while the second have an extremely limited orbit duration (also under 1 s), thus it can be attributed only a mathematical meaning.

Finally, solutions are divided by family on the basis of their orbit duration. Results are saved in a $.xlsx$, where each family is stored in a dedicated sheet, in the form of a $N_i \times 13$ matrix, where N_i is the number of identified solutions for the i^{th} family. The matrix is built according to the following structure: columns from 1 to 6 - contain the coordinates of the spacecraft-moon rendezvous and the vector components of the spacecraft velocity at the

encounter; column 7 contains to the duration of the orbit (in s); in column 8 is stored the value of α, while column 9 contains the initial angular position of the Sun (θ_{S_0}); columns 10 and 11 are dedicated to the angular position of both spacecraft and moon at the rendezvous (even though this means the same value is saved twice for each solution, this strategy has been used so as to have one more check regarding whether the rendezvous has been properly reached), column 12 contains the conversion of T_E in lunar months; the final column contains the angular position of the Sun at the moment of rendezvous.

After having classified the values of α that permit for a moon-to-moon transfer according to their duration, the corresponding orbits are drawn. Each family is given an accurate name, composed of three letters: the first one, from A to F, identifies the family according to the duration of the orbits, with A corresponding to $T_E \simeq 1\ month$, B to $T_E \simeq 2\ months$, and so on; the other two distinguish whether in the family are present outbound-inbound orbits or inbound-inbound ones. For instance, a family consisting of inbound-inbound orbits that allow a rendezvous after circa 5 months is classified as Eii.

In addition, a minimum altitude of 250 km is applied: if during the integration process the magnitude of the spacecraft's distance vector from Earth's centre achieves $R_\oplus + 250\ km$ or lower, integration is braked and a warning is showed. This allows accounting the dimensions of Earth and prevent both impacts and the feasible dissipation of energy due to drag caused by the atmosphere, which would stop the algorithm since has not been introduced a control on the conservation of mechanical energy.

3.2 Moon-to-escape lunar gravity assist

In order to study the LGA maneuver are used the results acquire during the moon-to-moon leg analysis: the spacecraft's position coordinates at the re-encounter, its velocity vector components, the value of α, the time of the encounter T_E (measured from the start of the integration process T_0), the angular position of the spacecraft at the encounter, the angular position of the Sun both at T_0 and at T_E, and the number of lunar revolutions between T_E and T_0.
Besides, to avoid collisions during the maneuver, the periselene r_p is fixed at 50 km over the moon's surface.

3.2.1 Lunar gravity assist evaluation

The evalutation is performed for only one orbit family at a time, selected at the time of running the executable, as to reduce the computing time; for each selected family every orbit are considered (outermost loop).
First of all, a system change is executed: from a Cartesian reference system to a reference system moving with the moon with the first axis along the Earth-moon direction, the second one perpendicular to the moon orbit plane, and the third one parallel to $\boldsymbol{V_M}$ (obtained with the right-hand rule); this changed is applied to velocity vector, thus obtaining $\boldsymbol{V_\infty^-}$:

$$\begin{cases} u_\infty^- = V_{\infty,X}\cos\theta + V_{\infty,Y}\sin\theta \\ v_\infty^- = -V_{\infty,X}\sin\theta + V_{\infty,Y}\cos\theta - V_M \\ w_\infty^- = 0 \end{cases} \tag{3.3}$$

Where θ, as exposed in section 3.1, is the angular position between the spacecraft and the moon at the re-encounter.
Moreover, given that the moon-to-moon leg stays on the moon orbit plane, the normal component of $\boldsymbol{V_\infty^-}$ is null.

Using the radial and tangential components of $\boldsymbol{V}_{\boldsymbol{\infty}}^{-}$, the pump angle at the start of the LGA maneuver can be evaluated:

$$p^{-} = \arctan \frac{u_{\infty}^{-}}{v_{\infty}^{-}} \tag{3.4}$$

After evaluating p^{-}, the maximum possible rotation (δ_{max}) that can be achieved by the LGA is calculated:

$$\delta_{max} = 2 \arcsin \frac{\mu_M / r_p}{V_{\infty}^{-2} + \mu_M / r_p} \tag{3.5}$$

Since $0 < \delta < \delta_{max}$, an inner loop begins where the possible pump angles after the LGA are taken into consideration:

$$p^{-} - \delta_{max} < p^{+} < p^{-} + \delta_{max} \tag{3.6}$$

After for every p^{+}, all probable crank angles after the LGA are evaluted, from 0 to the maximum value k_{max}^{+} (innermost loop), where k_{max}^{+} can be obtained from the definition of dot product:

$$\boldsymbol{V}_{\boldsymbol{\infty}}^{-} \cdot \boldsymbol{V}_{\boldsymbol{\infty}}^{+} = V_{\infty}^{2} \cos \delta \tag{3.7}$$

Writing the dot product (eq. 2.39) using pump and crank angles, and observing that $k^{-} = 0$:

$$\cos \delta = \cos p^{-} \cos p^{+} + \sin p^{-} \sin p^{+} \cos k^{+} \tag{3.8}$$

Remembering the limits for δ mentioned previously, it can be deduced that:

$$\cos \delta > \cos \delta_{max} \tag{3.9}$$

Therefore:

$$\sin p^{-} sin p^{+} \cos k^{+} > cos \delta_{max} - \cos p^{-} \cos p^{+} \tag{3.10}$$

Now, it is possible to identify two cases:

$$\begin{aligned} \sin p^{-} \sin p^{+} > 0 \quad &\longrightarrow \quad \cos k^{+} > \frac{\cos \delta - \cos p^{-} \cos p^{+}}{\sin p^{-} \sin p^{+}} \\ \sin p^{-} \sin p^{+} < 0 \quad &\longrightarrow \quad \cos k^{+} < \frac{\cos \delta - \cos p^{-} \cos p^{+}}{\sin p^{-} \sin p^{+}} \end{aligned} \tag{3.11}$$

The solution of the equation 3.11 is:

$$\cos k^+ = \frac{\cos\delta - \cos p^- \cos p^+}{\sin p^- \sin p^+} \tag{3.12}$$

Therefore:

$$k^+_{max} = \arccos\left(\frac{\cos\delta_{max} - \cos p^- \cos p^+}{\sin p^- \sin p^+}\right) \tag{3.13}$$

Where the argument of the arccosine function is denoted with arg :

$$arg = \frac{\cos\delta_{max} - \cos p^- \cos p^+}{\sin p^- \sin p^+} \tag{3.14}$$

Moreover, to assure k^+_{max} is correctly calculated, a verification is carried out both on the value arg that the sign of its denominator. It is to be highlighted that, for $k^+ = 0$ in equation 3.8:

$$\cos\delta = \cos p^- \cos p^+ + \sin p^- \sin p^+ = \cos|\Delta p| > \cos\delta_{max} \tag{3.15}$$

Therefore:

$$\begin{aligned} \sin p^- \sin p^+ > 0 \quad &\longrightarrow \quad arg < 1 \\ \sin p^- \sin p^+ < 0 \quad &\longrightarrow \quad arg > 1 \end{aligned} \tag{3.16}$$

There are only three feasible cases, as the others do not produce significant solutions:

- $\sin p^- \sin p^+ > 0,\ -1 < arg < 1 \longrightarrow\ k_{max}$ is calculated according to equation 3.13;
- $\sin p^- \sin p^+ > 0,\ arg < -1 \longrightarrow\ k_{max} = 180°$;
- $\sin p^- \sin p^+ < 0$ (i.e. the gravity assist manoeuvre modifies the sign of the pump angle) $\longrightarrow\ k_{max} = 180°$.

Using again equation 2.39, inside the innermost loop, the velocity relative to the moon after the LGA maneuver is computed for each k^+.

Afterwards, the absolute velocity in Earth's reference frame is got:

$$\begin{cases} u^+ = u_\infty^+ \\ v^+ = v_\infty^+ + V_M \\ w^+ = w_\infty^+ \end{cases} \tag{3.17}$$

To calculate the escape velocity, it is required to compute the energy associated to the orbit where is spacecraft.

$$\mathscr{E} = \frac{V^{+2}}{2} - \frac{\mu_E}{R_M} \tag{3.18}$$

Now, a further check is carried out, if the energy $\mathscr{E}$ is negative (i.e. the orbit is closed), the code is breaked and is moved to the next iteration; this is done because the aim of analysis is evaluate the evasion maneuvers.
Therefore, the characteristic energy can be computed:

$$C3 = 2\mathscr{E} \tag{3.19}$$

The magnitude of the escape velocity vector, supposing $r \to \infty$ at the escape, is:

$$V_{esc} = \sqrt{C3} \tag{3.20}$$

The other parameters of spacecraft's orbit can be obtained as shown below. The specific angular momentum is computed:

$$h = R_M \sqrt{v^{+2} + w^{+2}} \tag{3.21}$$

This value is used to calculate the orbital eccentricity, which should be greater than 1, since $\mathscr{E} > 0$:

$$e = \sqrt{1 + \frac{2\mathscr{E}h^2}{\mu_E^2}} \tag{3.22}$$

The evaluation of the semi-major axis is obtained form the equation 3.18 , which depend on the orbit size:

$$a = -\frac{\mu_E}{2\mathscr{E}} \tag{3.23}$$

Consequently, the semilatus rectum can be computed as:

$$p = a\left(1 - e^2\right) \tag{3.24}$$

Equally, the perigee can be calculated also:

$$r_p = a\left(1 - e\right) \tag{3.25}$$

Instead, the true anomaly, which identifies the position of the spacecraft on its hyperbolic orbit, can be achieved from equation 2.30:

$$\nu = \arccos\frac{p/R_M - 1}{e} \tag{3.26}$$

Its aperture is computed as followed:

$$\varphi = \arccos\frac{1}{e} \tag{3.27}$$

To avoid collisions with Earth, another verification is performed: if the true anomaly (ν) is negative, i.e. the spacecraft is close to the perigee, the perigee radius (achieved from equation 3.25) is compared to Earth's radius raised by 200 km; if r_p is under this value, the algorithm jumps to the next iteration and disregards the current solution.

Making geometric considerations on figure 3.2, it can now be estimated the angle between the direction corresponding to the true anomaly after the LGA and the direction of $\boldsymbol{V_{esc}}$:

$$\Delta = \pi - \varphi - \nu \tag{3.28}$$

The inclination of the escape orbit can be deduced from $\boldsymbol{V}^+$ components:

$$i = \arctan\frac{w^+}{v^+} \tag{3.29}$$

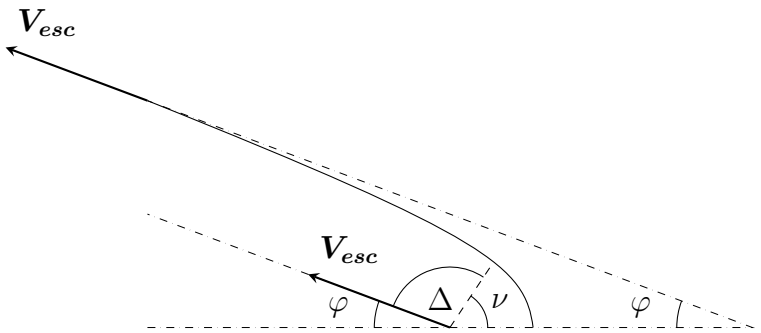

Figure 3.2: Geometrical schema for escape orbit.

Now, the angle Ω is introduced, which identify the angular position of the LGA relative to the sun's:

$$\Omega = \theta - \theta_S \tag{3.30}$$

Finally, another reference change is carried out, considering the effects of Δ, i, and Ω; this allow evalutating the components of the spacecraft's velocity ($\boldsymbol{V_H}$) in a radial-tangential-normal reference frame centered at the sun:

$$\begin{cases} \dfrac{u_H}{V_H} = \sin\Delta\sin\Omega\cos i - \cos\Delta\cos\Omega \\ \dfrac{v_H}{V_H} = -\sin\Delta\cos\Omega\cos i - \cos\Delta\sin\Omega \\ \dfrac{w_H}{V_H} = \sin\Delta\sin i \end{cases} \tag{3.31}$$

Underline that $V_{esc} = V_H$, since it is the same vector represented in two different reference systems.
Therefore, as illustrated in figure 3.3, the heliocentric flight-path angle (γ_H) and declination (δ_H) for the spacecraft's velocity after the LGA maneuver are computed:

$$\begin{cases} \gamma_H = \arctan\dfrac{u_H}{v_H} \\ \delta_H = \left|\arcsin\dfrac{w_H}{V_H}\right| \end{cases} \tag{3.32}$$

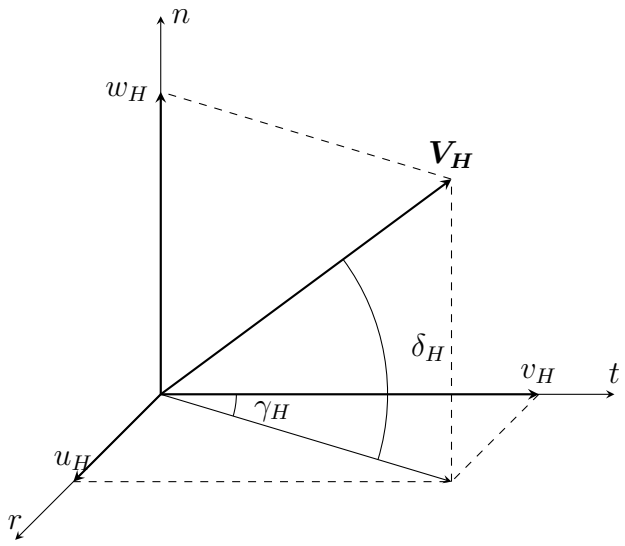

Figure 3.3: Heliocentric flight-path angle (γ_H) and declination (δ_H) for the spacecraft's velocity after the lunar gravity assist.

Note that in equation 3.32, δ_H is calculated using the modulus (i.e. the study is confined to positive values of declination) being the maneuver symmetrical: it is enough to invert k^+ to modify the sign of δ_H.

3.2.2 Maximum $C3$, given heliocentric flight-path angle and declination

The procedure described in section 3.2.1, for every of the solutions found for the moon-to-moon leg enable to build three matrices each one joining a value of $C3$, γ_H and δ_H respectively to a couple $(p^+,\ k^+)$. As the purpose of the study is to link $C3$ to γ_H and δ_H, the final part of the code interpolate data coming from the three matrices mentioned above: for every couple $(p^+,\ k^+)$ considered during the LGA evaluation, the corresponding values for $C3$ to γ_H and δ_H are acquired from the relative matrix, and the latter two are rounded to the closest integer. Thus, it can be written:

$$\begin{aligned} \gamma &\longrightarrow 0 \leq g \leq 359, \quad g \in \mathbb{N} \\ \delta &\longrightarrow 0 \leq d \leq 90, \quad d \in \mathbb{N} \end{aligned} \tag{3.33}$$

After, $(g+1)$ and $(d+1)$ are used as indices to created a matrix with the value of $C3$ corresponding to the γ_H and δ_H ($C3_{max}\,(g,\ d) \in \mathbb{R}^{360\times 91}$), for each family; if the couple $(g,\ d)$ repeats, the higher C3 is stored, while the lower one is put aside.

At the end, for a global evaluation, the twelve matrices obtained are assembled: for each $(g,\ d)$ couple, the values of $C3$ from each of the twelve families are compared and the maximum one among them is stored in a new matrix. The final result is a map which associates to a given γ_H and a given δ_H the maximum attainable energy value after the lunar gravity assist maneuver, regardless from the duration of the moon-to-moon leg.

Chapter 4

Results

4.1 Moon-to-moon leg

In this section, for three different spacecraft initial velocities relative to Moon ($V_\infty = 0.9$ Km/s,$V_\infty = 1$ Km/s e $V_\infty = 1.1$ Km/s) , the orbits allowing a rendezvous between the spacecraft and the moon are shown, for both outbound-inbound and inbound-inbound families.

4.1.1 Outbound-inbound

As regard outbound-inbound families (figure 4.1, 4.2 and 4.3), it is observed clearly that for a limited range of α, trajectories that allow a rendezvous between the spacecraft and the moon are identified. This range is influenced by both the family (i.e. the duration of the moon-to-moon leg) and spacecraft initial velocity relative to Moon.
For the first aspect, if a velocity $V_\infty = 1$ Km/s is considered, it is to be observed that while for *Aoi* family the interval in which solutions have been identified is limited to $\sim 4°$ ($110.50° - 114.75°$), *Foi* family displays a fivefold variation range ($87.81° - 108.52°$); the possible range of α where a solution can be found, becomes wider as the orbit duration increases. Moreover, it is to be noted how, for each family, the upper boundary of this interval stays close to 110°. Differently, the lower boundary of the range reduces constantly with the increase of T_E, meaning that the first LGA maneuver can have more

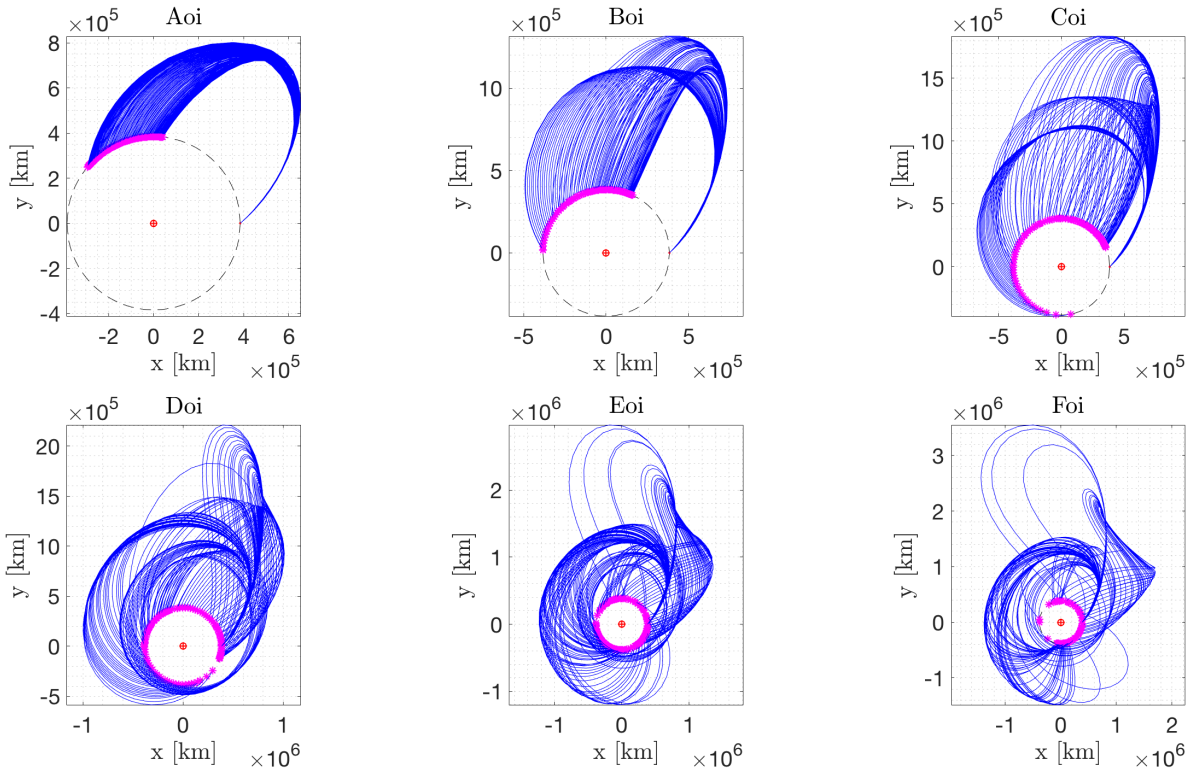

Figure 4.1: Outbound-inbound orbits for $V_\infty = 0.9$ Km/s. Initial and final positions of the moon are shown by red circles and magenta asterisks, respectively. The dashed circumference shows the lunar orbit around Earth, assumed circular.

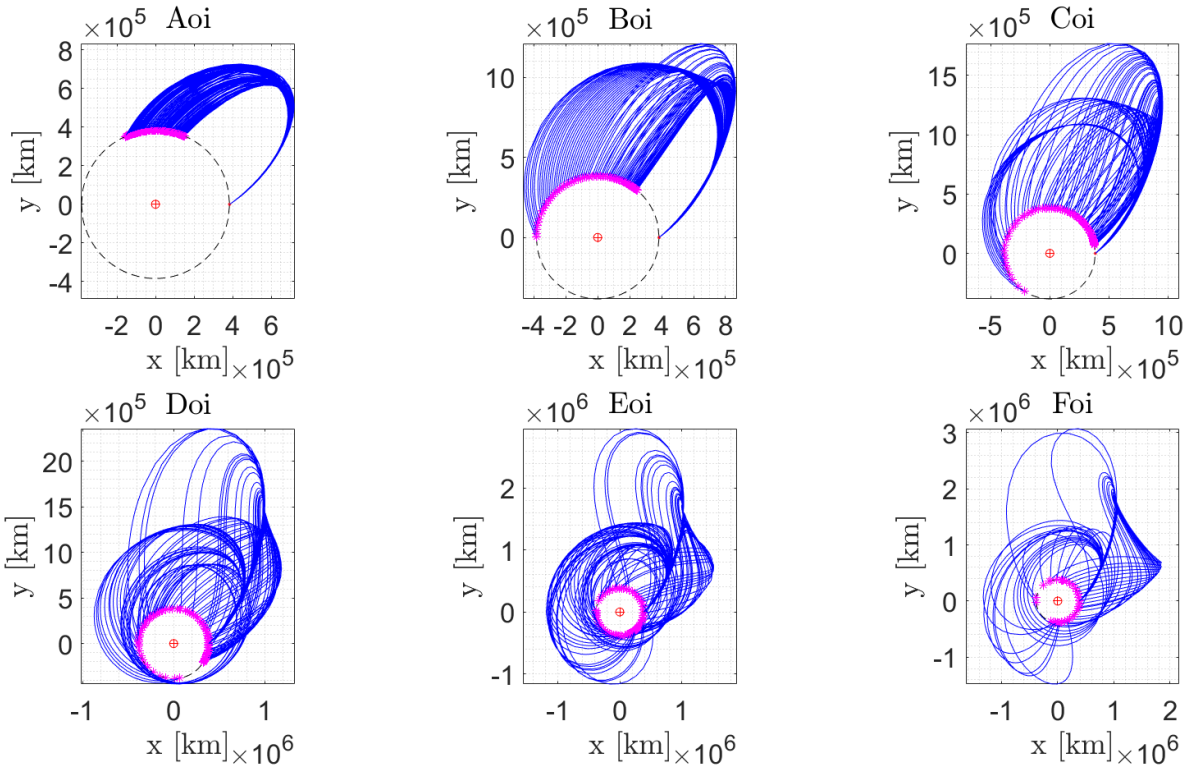

Figure 4.2: Outbound-inbound orbits for $V_\infty = 1$ Km/s. Initial and final positions of the moon are shown by red circles and magenta asterisks, respectively. The dashed circumference shows the lunar orbit around Earth, assumed circular.

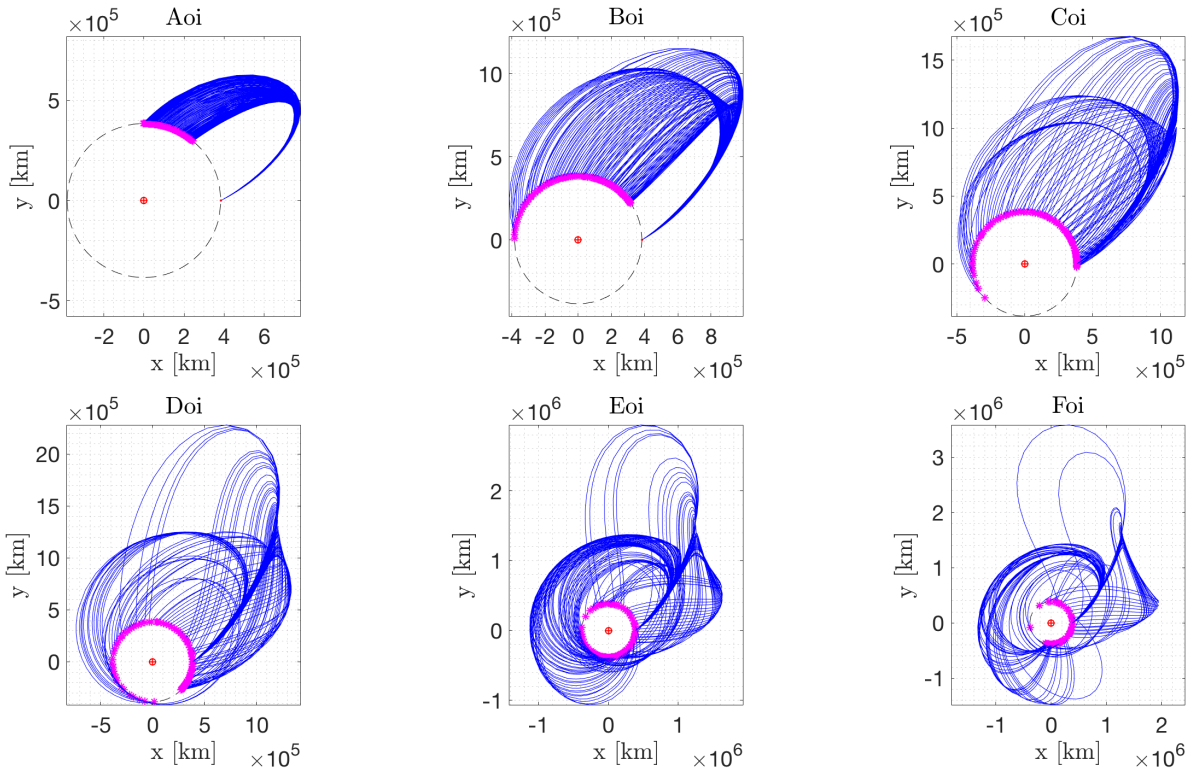

Figure 4.3: Outbound-inbound orbits for $V_\infty = 1.1$ Km/s. Initial and final positions of the moon are shown by red circles and magenta asterisks, respectively. The dashed circumference shows the lunar orbit around Earth, assumed circular.

Table 4.1: Ranges (in °) for α and θ_{SC} for oi families and $V_\infty = 0.9$ Km/s.

Family	α_{min}	α_{max}	α range	$\theta_{SC,min}$	$\theta_{SC,max}$	θ_{SC} range
Aoi	105.71	110.40	4.69	83.83	139.60	55.78
Boi	96.22	105.65	9.43	47.41	188.12	140.71
Coi	90.56	105.57	15.01	27.01	277.33	250.32
Doi	86.52	104.56	18.04	-21.24	322.58	343.82
Eoi	83.52	104.27	20.75	-188.15	167.76	355.9
Foi	81.15	104.20	23.05	-101.31	321.70	333.01

Table 4.2: Ranges (in °) for α and θ_{SC} for oi families and $V_\infty = 1$ Km/s.

Family	α_{min}	α_{max}	α range	$\theta_{SC,min}$	$\theta_{SC,max}$	θ_{SC} range
Aoi	110.50	114.75	4.25	66.95	114	47.05
Boi	101.40	109.93	8.53	50.22	178.84	128.62
Coi	96.22	109.63	13.41	9.71	243.94	234.23
Doi	92.59	108.86	16.27	-31.53	300.31	331.84
Eoi	89.92	108.81	18.89	-178.91	162.05	340.96
Foi	87.81	108.52	20.71	-109.19	217.51	326.70

Table 4.3: Ranges (in °) for α and θ_{SC} for oi families and $V_\infty = 1.1$ Km/s.

Family	α_{min}	α_{max}	α range	$\theta_{SC,min}$	$\theta_{SC,max}$	θ_{SC} range
Aoi	115.14	119.03	3.89	50.41	90.68	40.27
Boi	106.27	114.05	7.78	51.93	170.27	118.34
Coi	101.43	113.46	12.04	2.61	220.75	218.14
Doi	98.11	112.96	14.85	-44.18	272.68	316.86
Eoi	95.67	112.71	17.04	-185.39	148.01	333.4
Foi	93.76	112.64	18.88	-105.28	192.22	297.5

solutions that result practicable for a moon-to-moon trajectory.

For the second aspect, is observed that as the velocity increases, the values of α_{max} and α_{min} increase for each family, while the range of α is reduced.

Besides the considerations made on the range of α, another important aspect is the location of the rendezvous θ_{SC}: in comparison to Aoi, Boi, and Coi families, the last families allow re-encounters almost all along moon's orbit, having a larger range of α and a greater time available. This begins to be possible even for the Coi family, going to increase spacecraft initial velocity relative to Moon.

Finally, another noteworthy aspect is the perturbative effect of the Sun on the spacecraft orbit: long-lasting orbits that reach significant distances from Earth revel remarkable irregularities that are not according to with a Newtonian description of the orbital motion, while shorter legs appear to be more regular and without inversions – although the orbits are not simply conic in these cases.

4.1.2 Inbound-inbound

Similar considerations to the ones made on oi families are applicable inbound-inbound orbits, shown in figure 4.4, 4.5 and 4.6.

The range of α once again rises with the duration of the orbit while it decreases with increasing V_∞, in a similar way to what has been seen for oi families. The upper and lower boundaries change their role, meaning that, considering a $V_\infty = 1$ Km/s, for inbound-inbound orbits the lower boundary is the one presenting the less amount of variation (from $-120.65°$ for Aii to $-108.58°$ for Fii) in comparison to the higher boundary (from $-117.84°$ to $-87.86°$) and this does not change for different V_∞. This role change, though, is logical and expected: as observed by oi families longer-lasting orbits allow values of α determining a $\boldsymbol{V_\infty}$ closer to $\boldsymbol{V_M}$, in comparison to shorter ones.

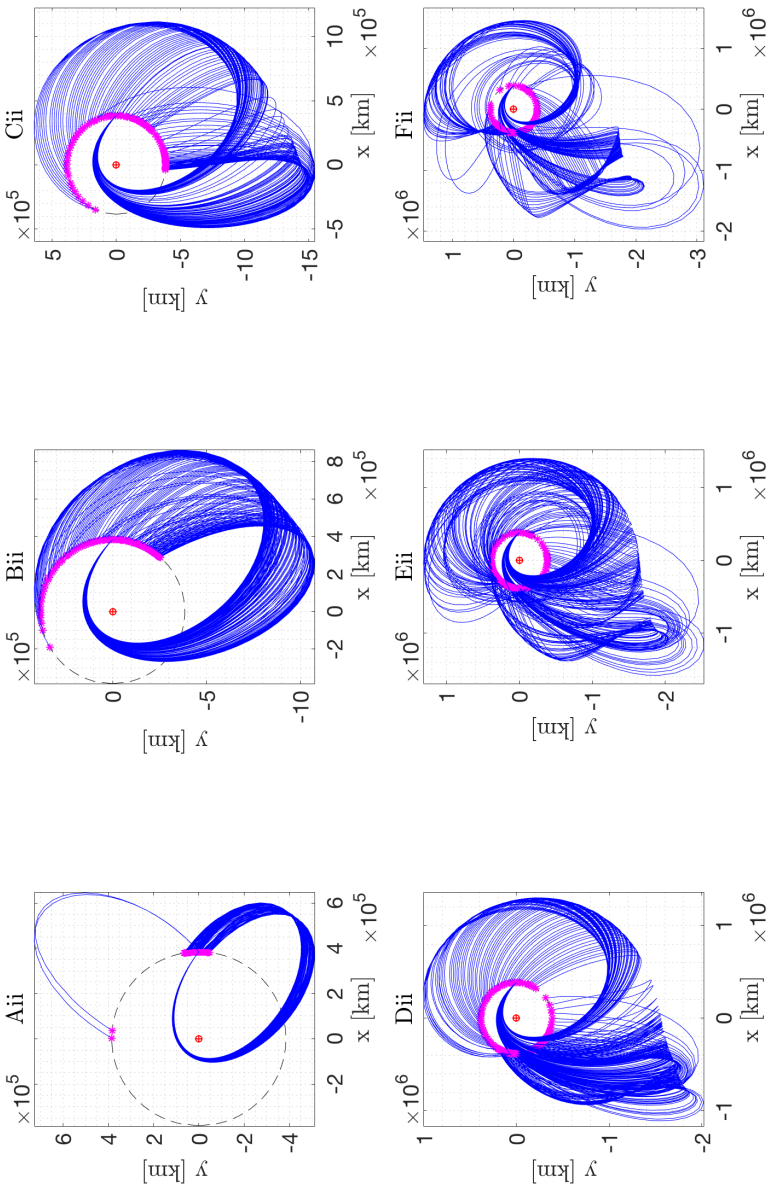

Figure 4.4: Inbound-inbound orbits $V_\infty = 0.9$ Km/s. Initial and final positions of the moon are shown by red circles and magenta asterisks, respectively. The dashed circumference shows the lunar orbit around Earth, assumed circular.

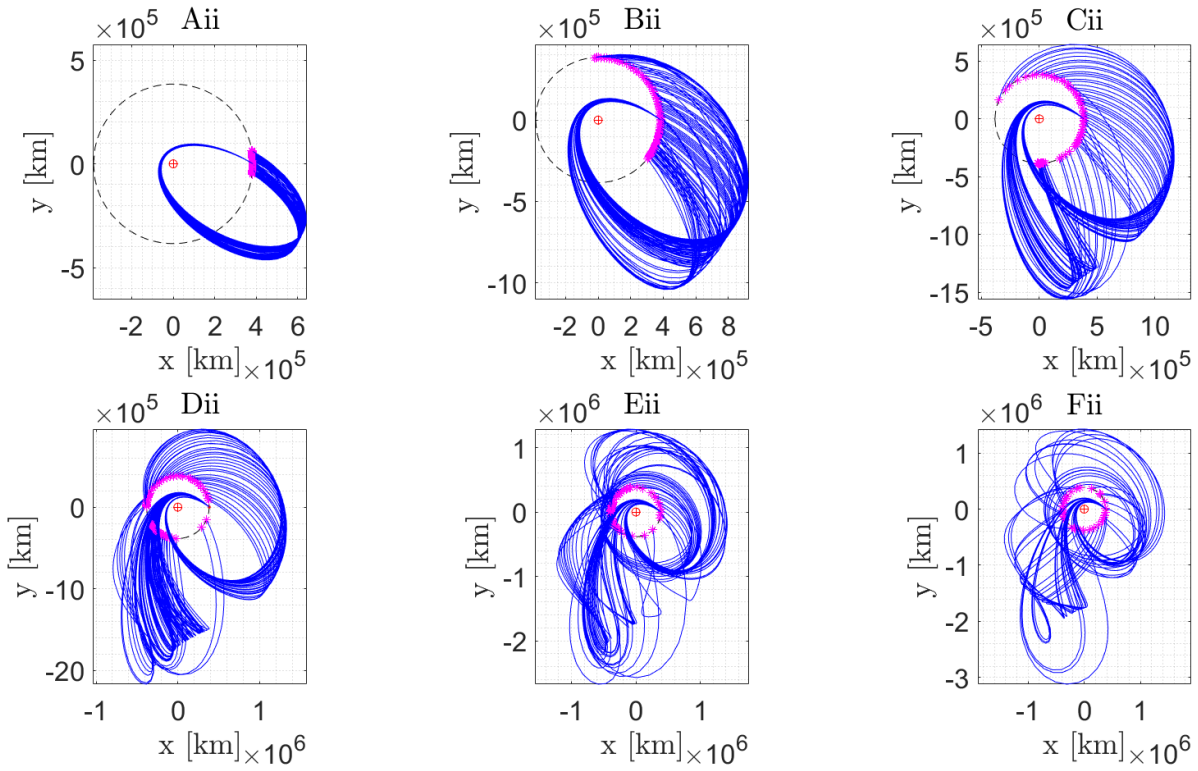

Figure 4.5: Inbound-inbound orbits$V_\infty = 1$ Km/s. Initial and final positions of the moon are shown by red circles and magenta asterisks, respectively. The dashed circumference shows the lunar orbit around Earth, assumed circular.

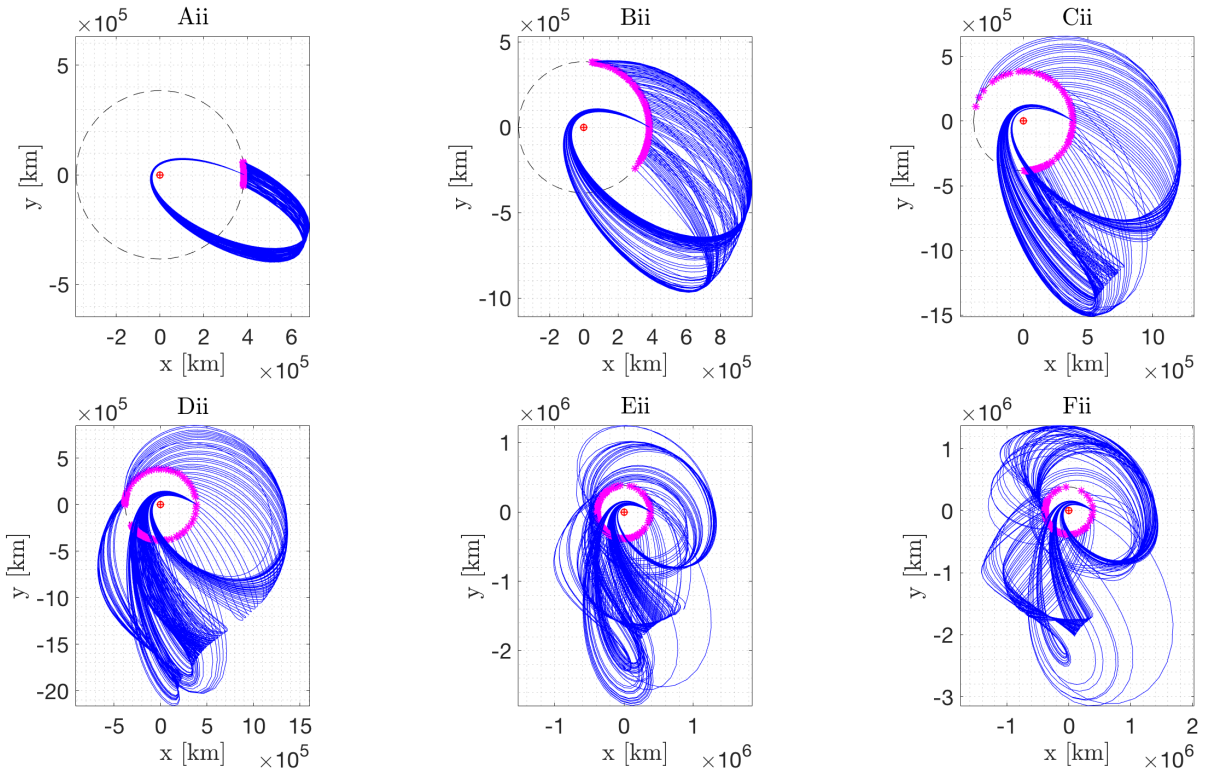

Figure 4.6: Inbound-inbound orbits $V_\infty = 1.1$ Km/s. Initial and final positions of the moon are shown by red circles and magenta asterisks, respectively. The dashed circumference shows the lunar orbit around Earth, assumed circular.

Table 4.4: Ranges (in °) for α and θ_{SC} for ii families and $V_\infty = 0.9$ Km/s.

Family	α_{min}	α_{max}	α range	$\theta_{SC,min}$	$\theta_{SC,max}$	θ_{SC} range
Aii	-117.62	-114.67	2.95	-6.79	9.26	16.05
Bii	-107.78	-100.75	7.03	-38.21	226.84	155.05
Cii	-105.10	-94.08	11.02	-99.98	159.17	259.15
Dii	-104.48	-87.07	17.41	-33.40	313.43	346.83
Eii	-104.36	-83.58	20.78	-27.40	319.8	347.2
Fii	-104.27	-81.07	23.20	-40.55	284.81	325.36

Table 4.5: Ranges (in °) for α and θ_{SC} for ii families and $V_\infty = 1$ Km/s.

Family	α_{min}	α_{max}	α range	$\theta_{SC,min}$	$\theta_{SC,max}$	θ_{SC} range
Aii	-120.65	-117.84	2.80	-6.92	8.97	15.89
Bii	-111.40	-104.94	6.46	-39.94	95.45	135.39
Cii	-109.25	-98.82	10.43	-88.47	163.42	251.9
Dii	-108.75	-93.00	15.75	-156.04	179.97	336.01
Eii	-108.62	-90.00	18.62	84.84	254.85	337.69
Fii	-108.58	-87.86	20.72	-42.3	274.89	317.19

Table 4.6: Ranges (in °) for α and θ_{SC} for ii families and $V_\infty = 1.1$ Km/s.

Family	α_{min}	α_{max}	α range	$\theta_{SC,min}$	$\theta_{SC,max}$	θ_{SC} range
Aii	-120.97	-123.46	2.49	-7.16	8.58	15.74
Bii	-115.26	-109.02	6.24	-38.82	82.77	121.59
Cii	-113.18	-103.37	9.81	-83.59	157.64	241.23
Dii	-112.70	-98.36	14.34	-144.88	180.81	323.69
Eii	-112.57	-95.49	17.07	-73	256.58	329.58
Fii	-112.59	-94.85	17.74	-38.11	257.3	295.41

As for oi families, even for these families the location of rendezvous is an important aspect, since the shift from a small interval for the first families to the almost complete lunar orbit is even more evident. For example, always considering $V_\infty = 1$ Km/s, the family *Aii* presents a θ_{SC} at the re-encounter varying in a limited $\sim 16°$ interval around $0°$, even smaller than the $\sim 47°$ range for *Aoi*.

Finally, the perturbation due to the gravitational effect of the Sun is once again much evident for the last families, where the same irregularities and inversions of oi families are showing.

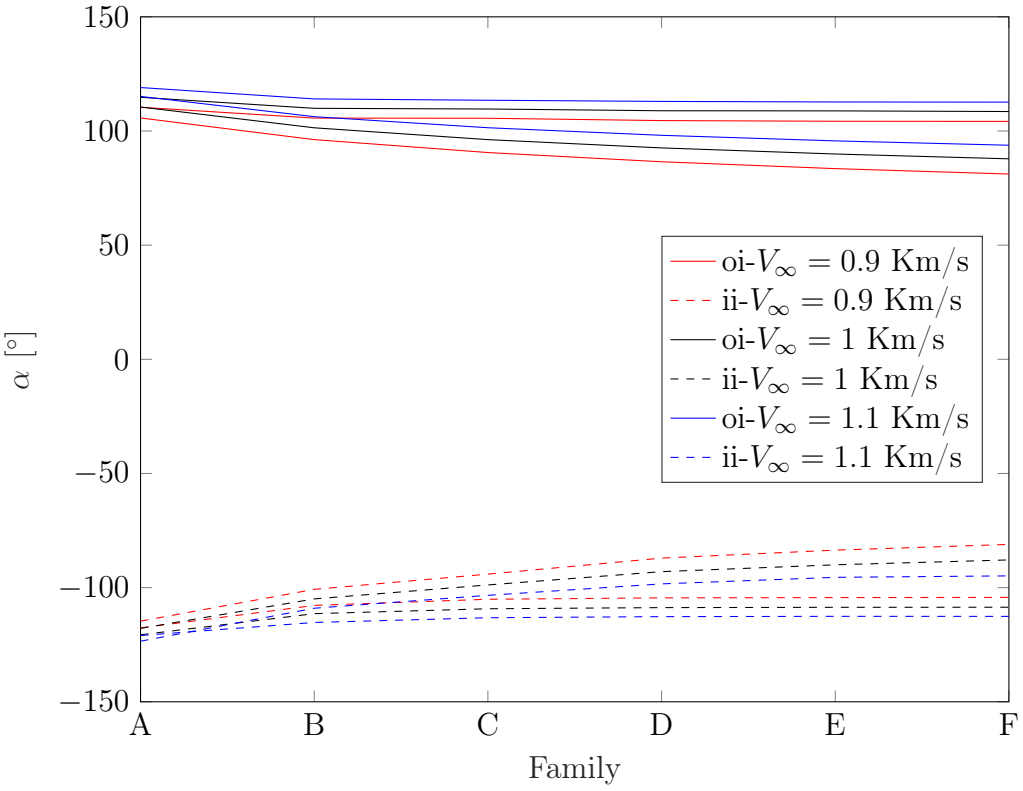

Figure 4.7: Range of α that allow a rendezvous for oi and ii families.

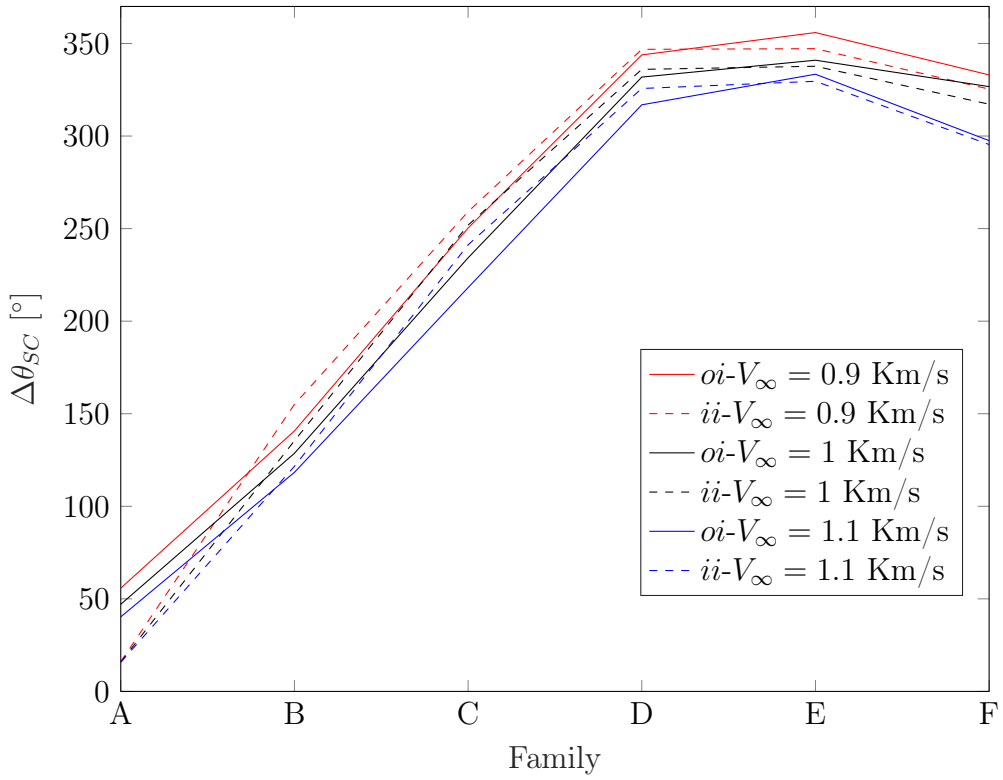

Figure 4.8: Range of θ that allow a rendezvous for oi and ii families.

4.2 Lunar gravity assist

In this section, the graphs where $C3(\gamma)$ is compared for different values of declination δ and for different spacecraft initial velocities relative to Moon ($V_\infty = 0.9$ Km/s,$V_\infty = 1$ Km/s e $V_\infty = 1.1$ Km/s) are shown.

4.2.1 $C3(\gamma)$ for given δ

Figures from 4.9 to 4.44 show the values for the maximum achievable characteristic energy $C3$ with varying flight-path angle γ, for fixed values of declination ($\delta = [0\ 30\ 45\ 60\ 80]$). Due to the nature of the perturbation effect generated by the Sun, all graphs show a periodicity around 180°, however, from A to C families clearly show this, compared last families. Therefore, considerations can be limited to $\gamma \in [0°, 180°]$. Furthermore, it can be highlighted that higher values for characteristic energy ($C3$) are generally limited to reduced declinations, independently of the family - although values themselves tend to vary and grew with longer-lasting orbits.

Aoi − Aii

Figures from 4.9 to 4.14 show that A families have a peak $C3$ around $\gamma = 70°$ and it is lightly higher for the outbound-inbound family, for the same V_∞; instead, as the velocity increases, this peak is had at higher $C3$.
Furthermore, it can be observed how escape manoeuvres are allowed only for low declination over the ecliptic plane. For instance, $\delta \geq 45°$ is not achievable if an escape associated to a moon-to-moon leg of ~ 1 month and $V_\infty \leq 1$ Km/s is desired, and even for $\delta = 30°$ escape trajectories are possible only for a limited range of flight-path angle, which increases with V_∞.
A particular feature of the curve for $\delta = 0°$ is its amplitude: considering $V_\infty = 1$ Km/s, while *Aoi* shows a higher peak, it also goes down to 1 km^2/s^2, whereas for *Aii* it does not reach 2 km^2/s^2 but it does not dip below 1.5 km^2/s^2; changing V_∞ this behaviour remains the same and only

the values of the maximum and minimum C3 will be changed. Therefore, *Aii* family seems to give a more consistent escape for each flight-path angle.

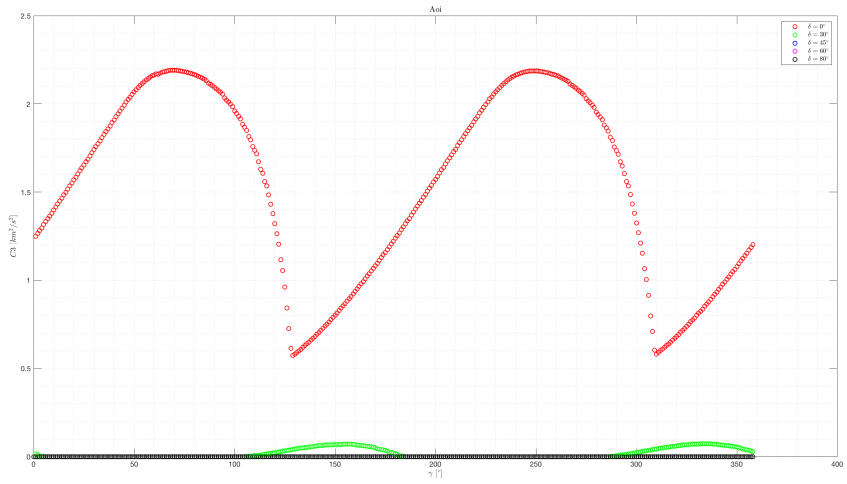

Figure 4.9: $C3_{max}$ function of the flight-path angle (γ) for fixed values of declination (δ) and $V_\infty = 0.9$ Km/s, *Aoi* family.

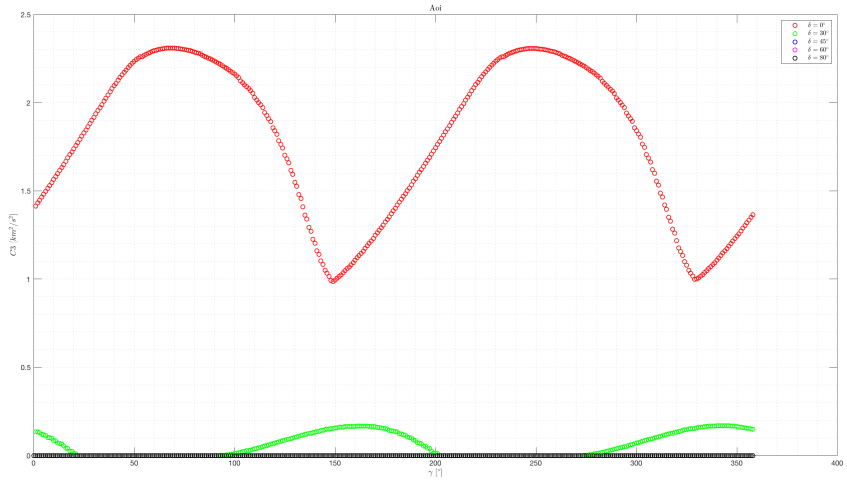

Figure 4.10: $C3_{max}$ function of the flight-path angle (γ) for fixed values of declination (δ) and $V_\infty = 1$ Km/s, *Aoi* family.

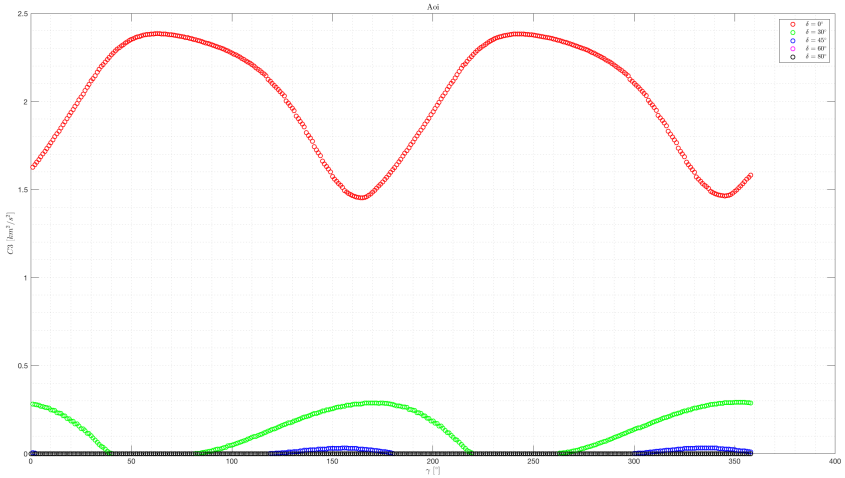

Figure 4.11: $C3_{max}$ function of the flight-path angle (γ) for fixed values of declination (δ) and $V_\infty = 1.1$ Km/s, *Aoi* family.

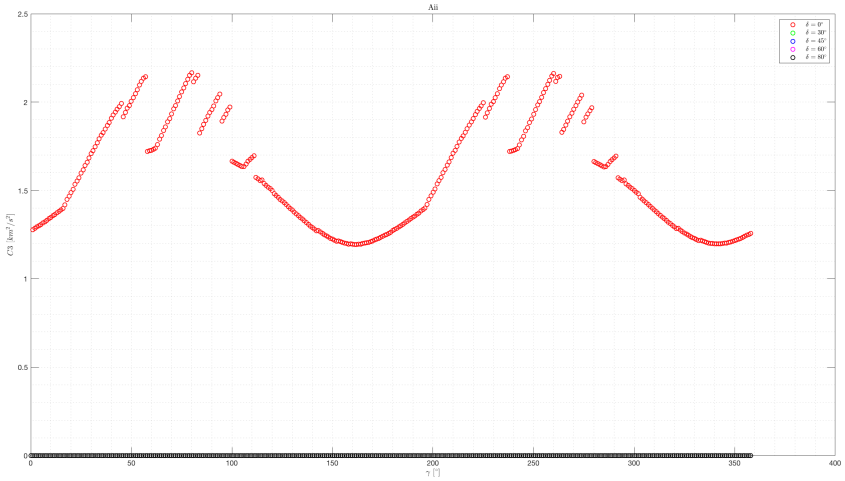

Figure 4.12: $C3_{max}$ function of the flight-path angle (γ) for fixed values of declination (δ) and $V_\infty = 0.9$ Km/s, *Aii* family.

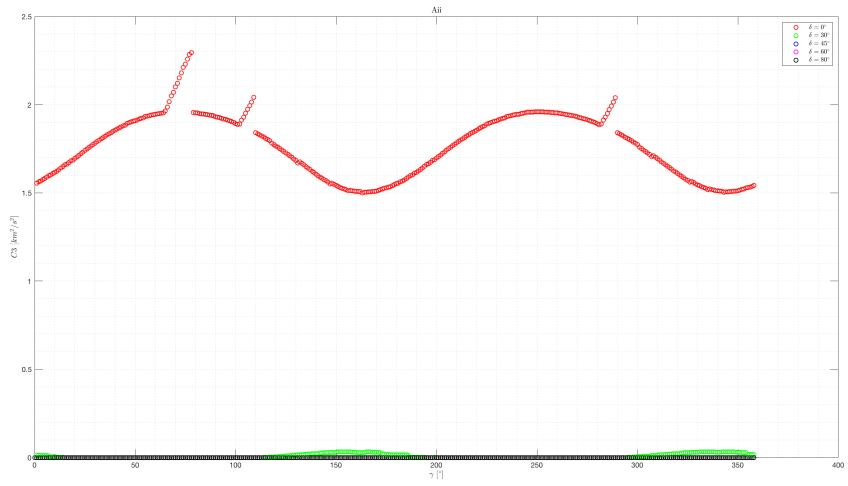

Figure 4.13: $C3_{max}$ function of the flight-path angle (γ) for fixed values of declination (δ) and $V_\infty = 1$ Km/s, *Aii* family.

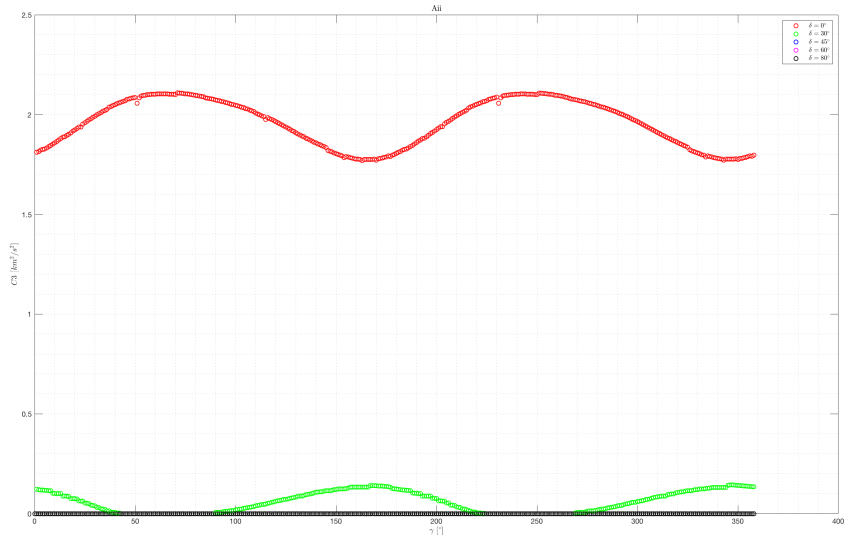

Figure 4.14: $C3_{max}$ function of the flight-path angle (γ) for fixed values of declination (δ) and $V_\infty = 1.1$ Km/s, *Aii* family.

Boi − Bii

Figures from 4.15 to 4.20 show that *Boi* family allows the achievement of higher characteristic energies compared to *Aoi*. Also, in this case, higher values is had for low declination, however, two peaks can be identified instead of a single one: a first, more evident one for $\gamma \simeq 50°$; then, a second, more difficult to identify just after $\gamma \simeq 100°$. *Boi* is continuous between the two peaks, showing a discontinuity for $\gamma \simeq 120°$, while *Bii* presents a jump both for $\gamma \simeq 120°$ and for $\gamma \simeq 55°$, between the maximums, but this discontinuity disappears for low velocities. Moreover, also for these families an increase of C3 is observed with the V_∞ .
Another noteworthy feature of these curves is the decrease of $C3$ with δ: more evident moving to flight-path angles corresponding to the maximums of the curves, whereas the variation is much more small when in the range of values of γ associated with minimum $C3$.
Additionally, it can be noted how multiple peaks are present only for $\delta = 0°$, whereas higher declination has a single maximum. Finally, another characteristic showed by the maximums is a shift to smaller flight- path angles: considering *Boi*, while the peak for $C3(\delta = 30°)$ is associated with $\gamma \simeq 200°$, the one for $\delta = 60°$ is before $\gamma = 180°$.

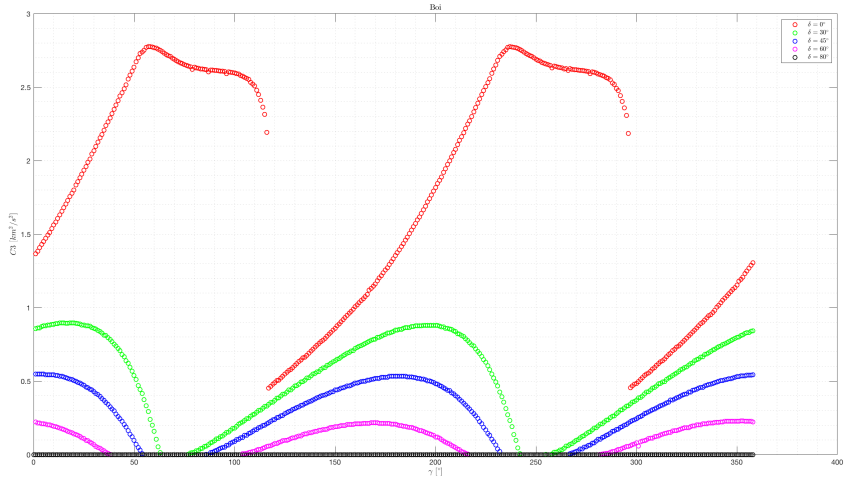

Figure 4.15: $C3_{max}$ function of the flight-path angle (γ) for fixed values of declination (δ) and $V_\infty = 0.9$ Km/s, *Boi* family.

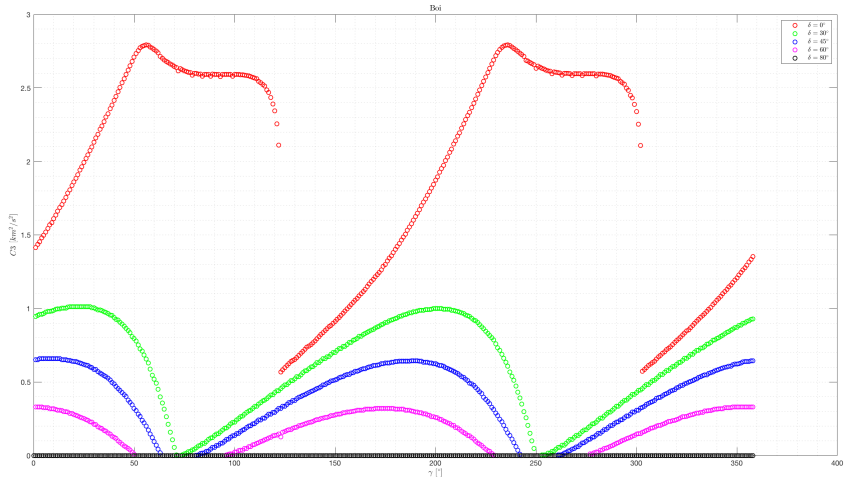

Figure 4.16: $C3_{max}$ function of the flight-path angle (γ) for fixed values of declination (δ) and $V_\infty = 1$ Km/s, *Boi* family.

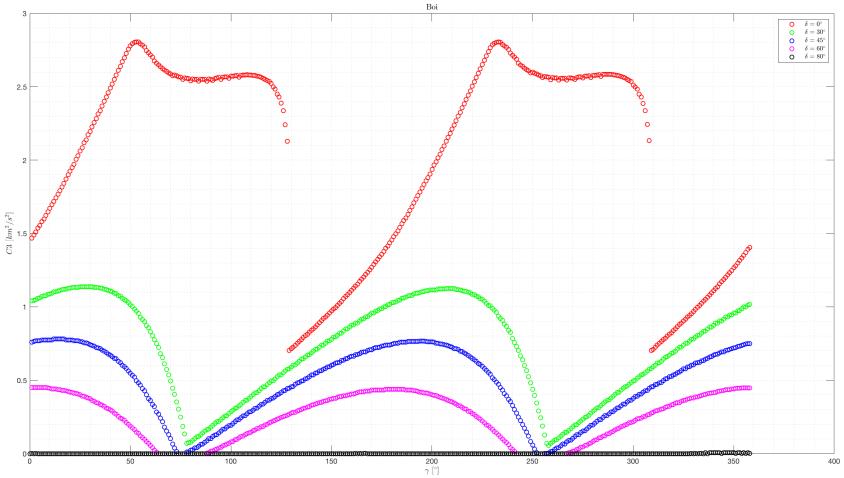

Figure 4.17: $C3_{max}$ function of the flight-path angle (γ) for fixed values of declination (δ) and and $V_\infty = 1.1$ Km/s, *Boi* family.

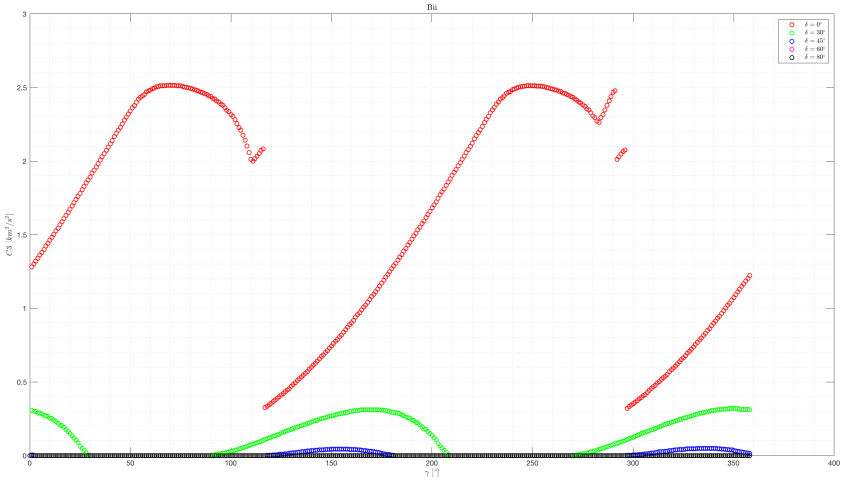

Figure 4.18: $C3_{max}$ function of the flight-path angle (γ) for fixed values of declination (δ) and $V_\infty = 0.9$ Km/s, *Bii* family.

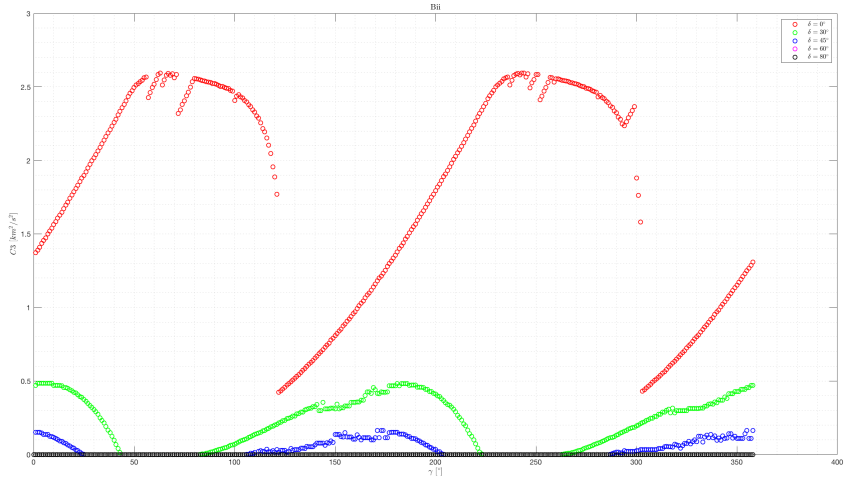

Figure 4.19: $C3_{max}$ function of the flight-path angle (γ) for fixed values of declination (δ) and $V_\infty = 1$ Km/s, *Bii* family.

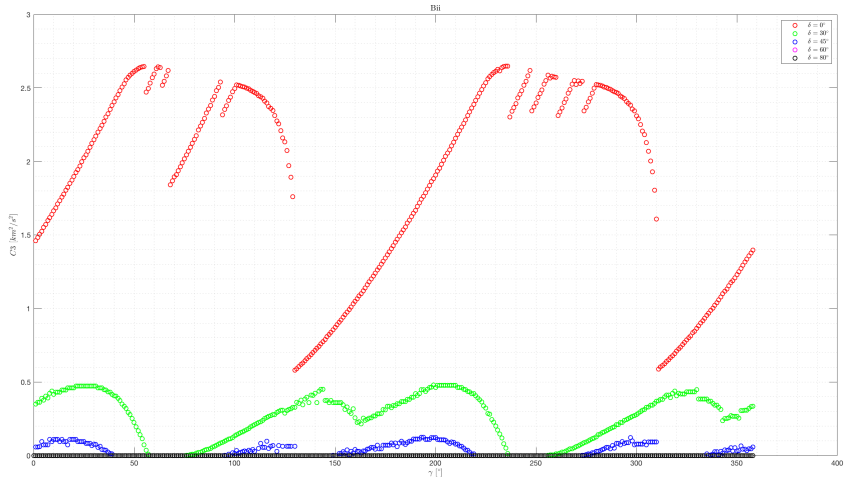

Figure 4.20: $C3_{max}$ function of the flight-path angle (γ) for fixed values of declination (δ) and $V_\infty = 1.1$ Km/s, *Bii* family.

$Coi - Cii$

If escapes with high declination for any γ are desired, accepting transfers of approximately 3 months or longer is necessary. As said previously, characteristic energy is higher than what is achievable with shorter moon-to-moon legs and inbound-inbound orbits seem to permit less energetic escapes respect to outbound-inbound.
Equally to B families, C families show multiple peaks as well, instead of a single one, and they are more spaced out. As for Boi, the multiple peaks that there are for null declination do not reach the same value, since the second one is more than 0.3 km^2/s^2 below the first one.
Moreover, it is visible how the distance between the maximum $C3$ for Coi and Cii is reduced compared to B families – and even more, if A families are taken into account. Finally, as in the previous families, C3 increases with V_∞.

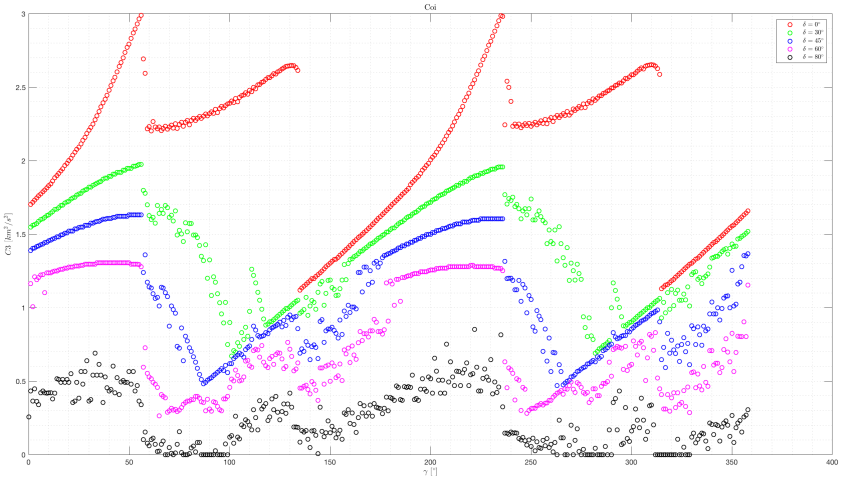

Figure 4.21: $C3_{max}$ function of the flight-path angle (γ) for fixed values of declination (δ)and $V_\infty = 0.9$ Km/s, *Coi* family.

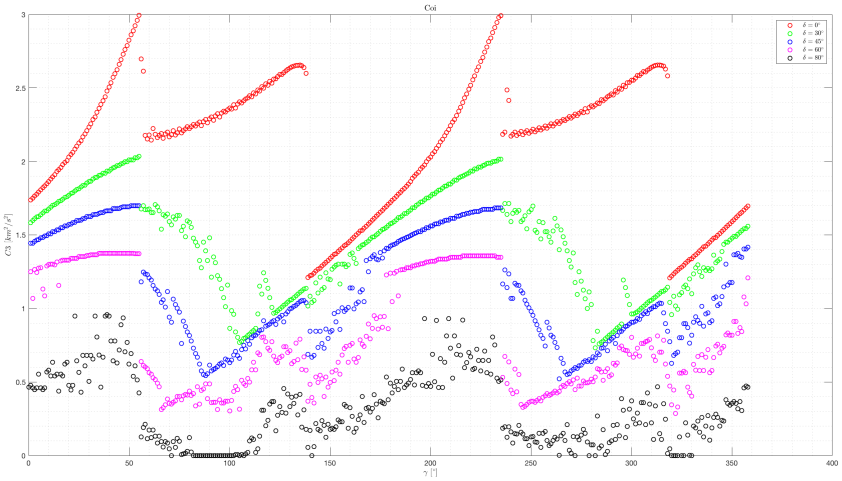

Figure 4.22: $C3_{max}$ function of the flight-path angle (γ) for fixed values of declination (δ) and $V_\infty = 1$ Km/s, *Coi* family.

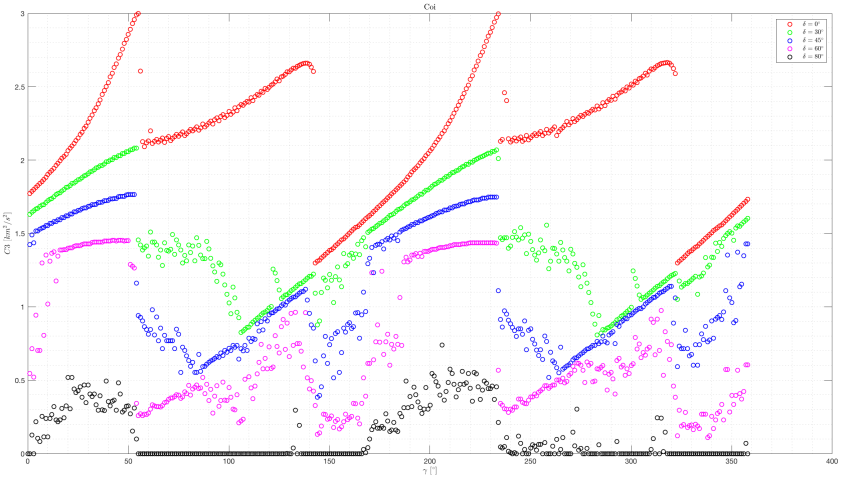

Figure 4.23: $C3_{max}$ function of the flight-path angle (γ) for fixed values of declination (δ) and $V_\infty = 1.1$ Km/s, *Coi* family.

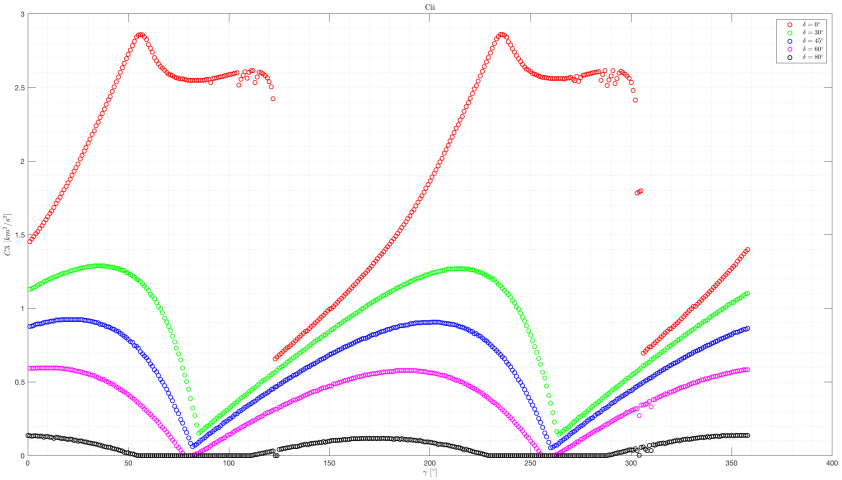

Figure 4.24: $C3_{max}$ function of the flight-path angle (γ) for fixed values of declination (δ) and $V_\infty = 0.9$ Km/s, *Cii* family.

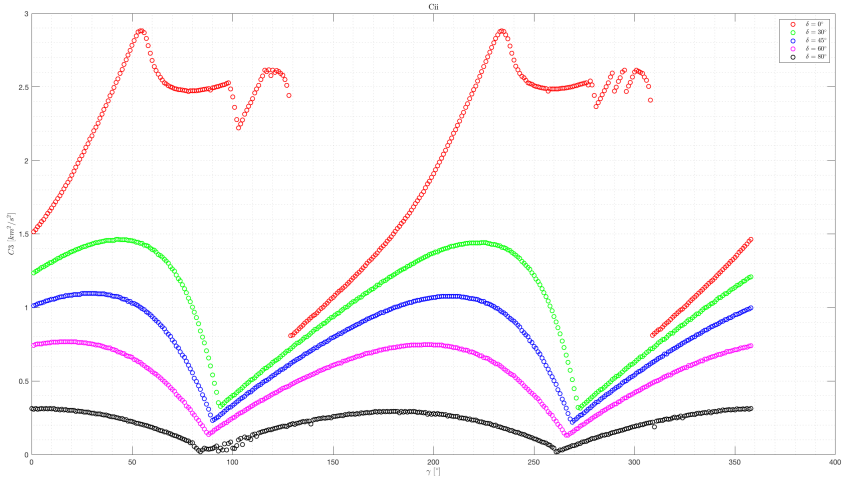

Figure 4.25: $C3_{max}$ function of the flight-path angle (γ) for fixed values of declination (δ) and $V_\infty = 1$ Km/s, *Cii* family.

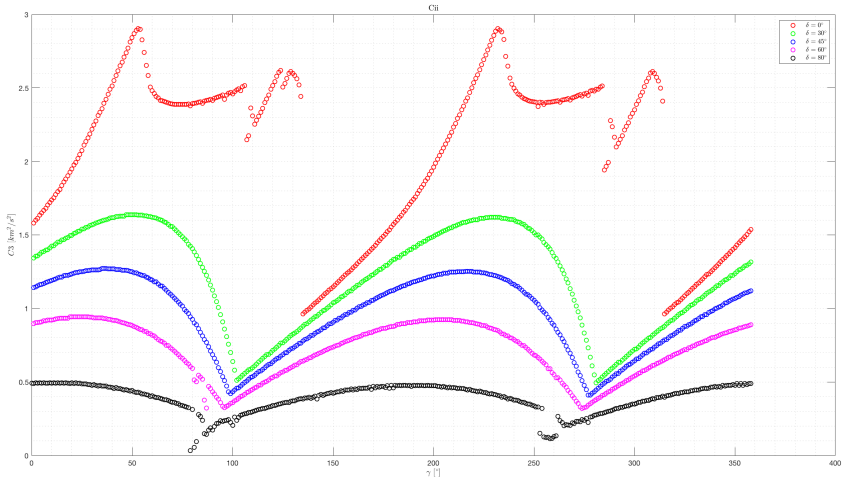

Figure 4.26: $C3_{max}$ function of the flight-path angle (γ) for fixed values of declination (δ) and $V_\infty = 1.1$ Km/s, *Cii* family.

Doi − Dii

Figures from 4.27 to 4.32 clearly show the curves are less regular than the previous families, but the symmetry continues to exist. While less apparent for $\delta = 0°$, higher declination angles see curves for $C3$ with multiple irregularites. Furthermore, the same considerations can be made on the C3-V_∞ ratio, made for previous families.

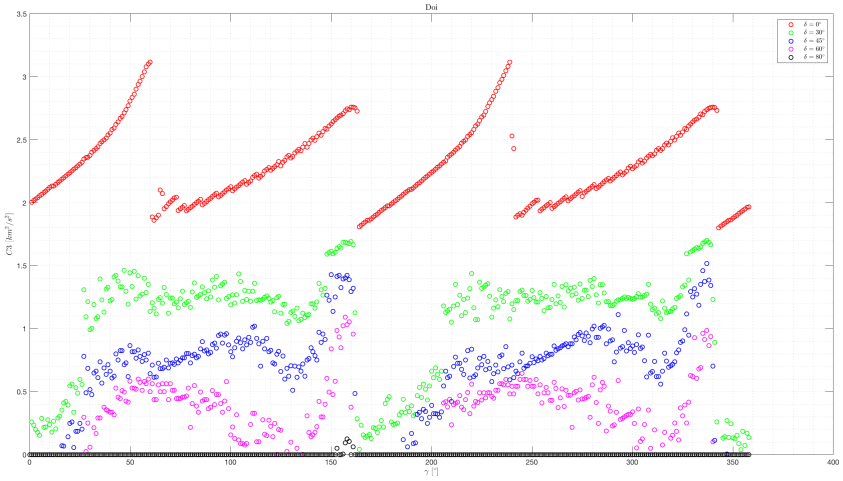

Figure 4.27: $C3_{max}$ function of the flight-path angle (γ) for fixed values of declination (δ) and $V_\infty = 0.9$ Km/s, *Doi* family.

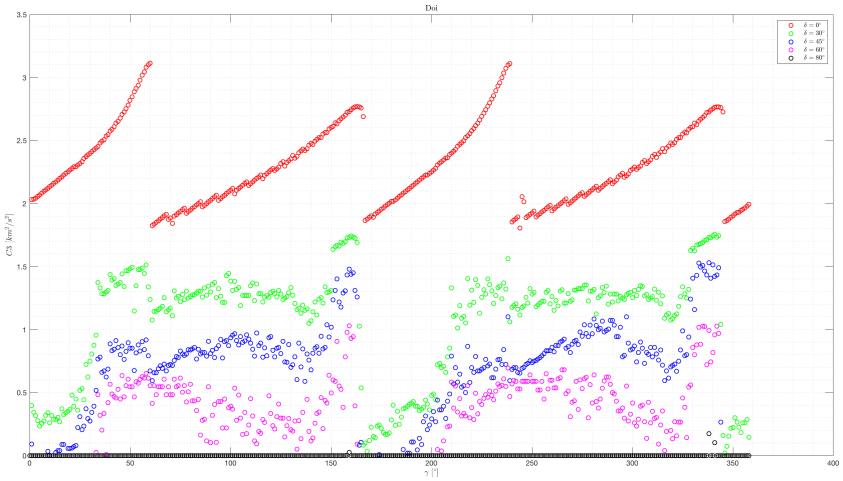

Figure 4.28: $C3_{max}$ function of the flight-path angle (γ) for fixed values of declination (δ) and $V_\infty = 1$ Km/s, *Doi* family.

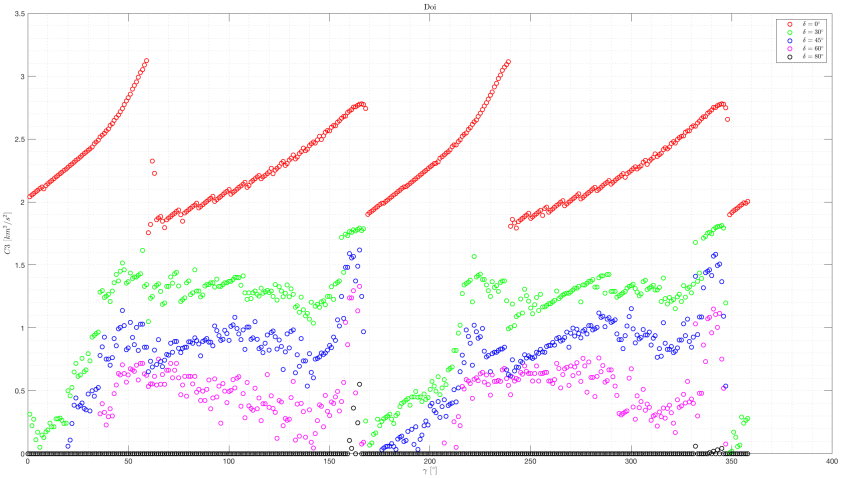

Figure 4.29: $C3_{max}$ function of the flight-path angle (γ) for fixed values of declination (δ) and $V_\infty = 1.1$ Km/s, *Doi* family.

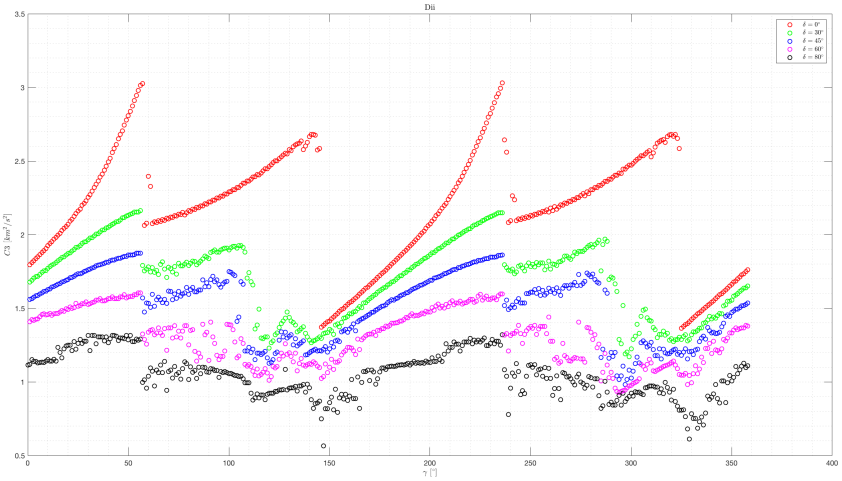

Figure 4.30: $C3_{max}$ function of the flight-path angle (γ) for fixed values of declination (δ) and $V_\infty = 0.9$ Km/s, *Dii* family.

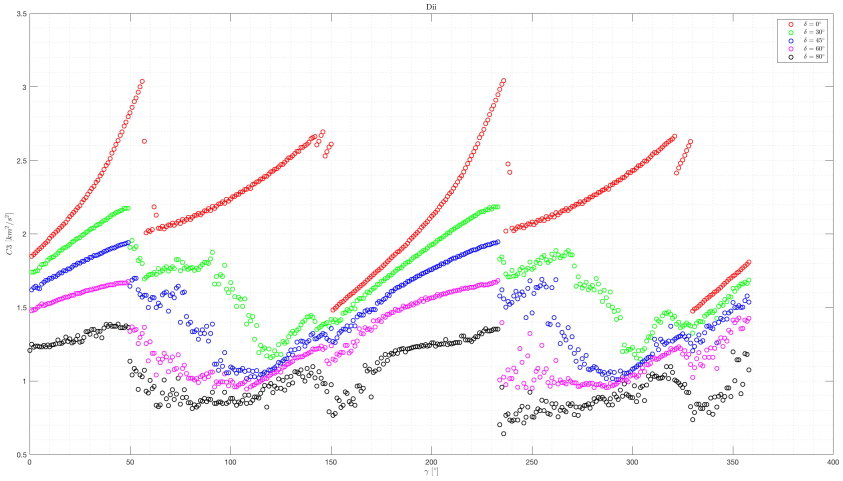

Figure 4.31: $C3_{max}$ function of the flight-path angle (γ) for fixed values of declination (δ) and $V_\infty = 1$ Km/s, *Dii* family.

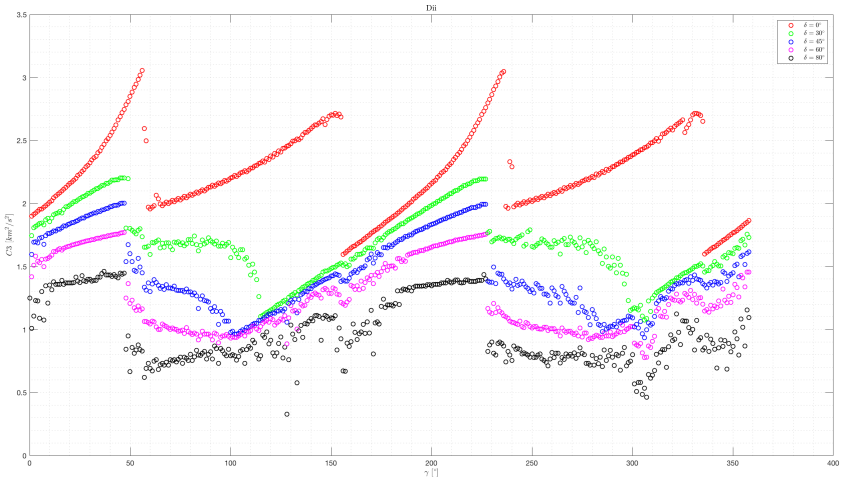

Figure 4.32: $C3_{max}$ function of the flight-path angle (γ) for fixed values of declination (δ) and $V_\infty = 1.1$ Km/s, *Dii* family.

Eoi − Eii

Similar observations to the ones for earlier families is done for E family: peak $C3$ rises and is higher for outbound-inbound orbits compared to inbound-inbound. However, the difference between oi and ii families are less evident, and ii orbits seem to be more and more similar to oi, in terms of escape conditions.
The difference between the outbound-inbound peak and the inbound-inbound one is reduced to the minimum, as both reach $C3 \simeq 3.2\ km^2/s^2$ – with Eii just lightly inferior.

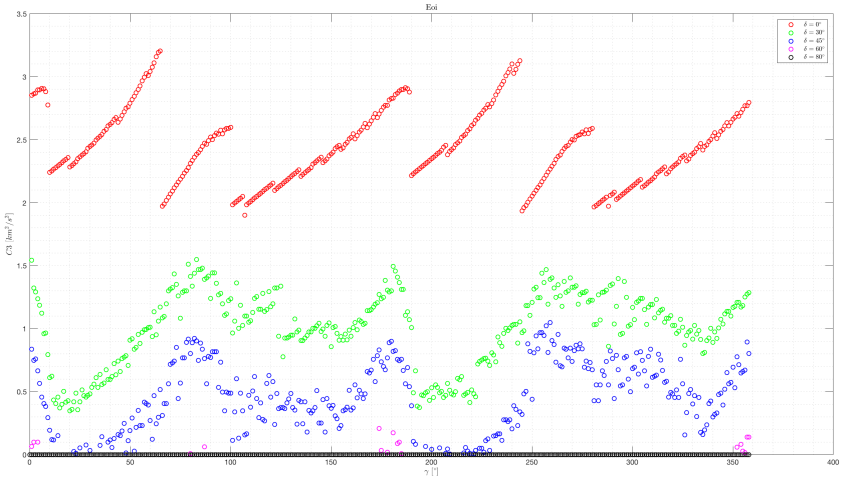

Figure 4.33: $C3_{max}$ function of the flight-path angle (γ) for fixed values of declination (δ) and $V_\infty = 0.9$ Km/s, *Eoi* family.

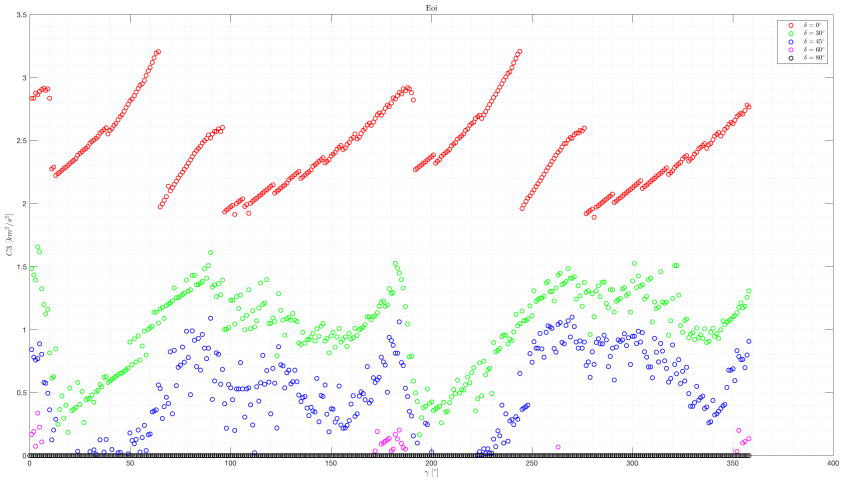

Figure 4.34: $C3_{max}$ function of the flight-path angle (γ) for fixed values of declination (δ) and $V_\infty = 1$ Km/s, *Eoi* family.

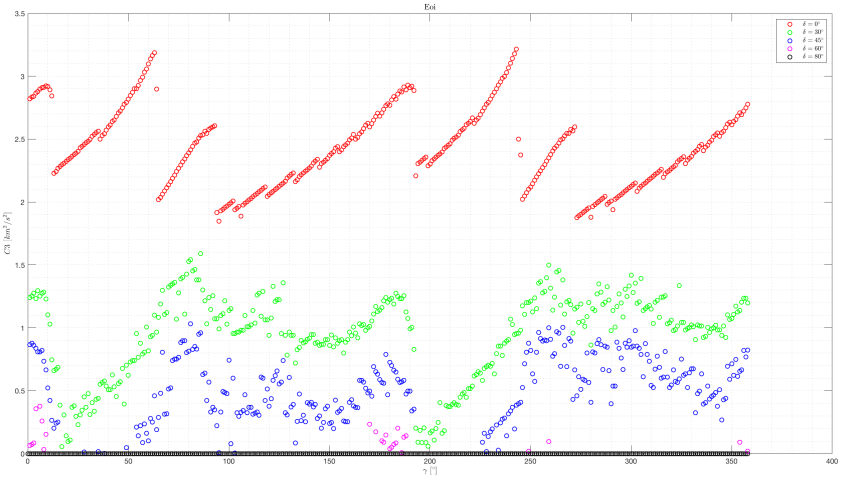

Figure 4.35: $C3_{max}$ function of the flight-path angle (γ) for fixed values of declination (δ) and $V_\infty = 1.1$ Km/s, *Eoi* family.

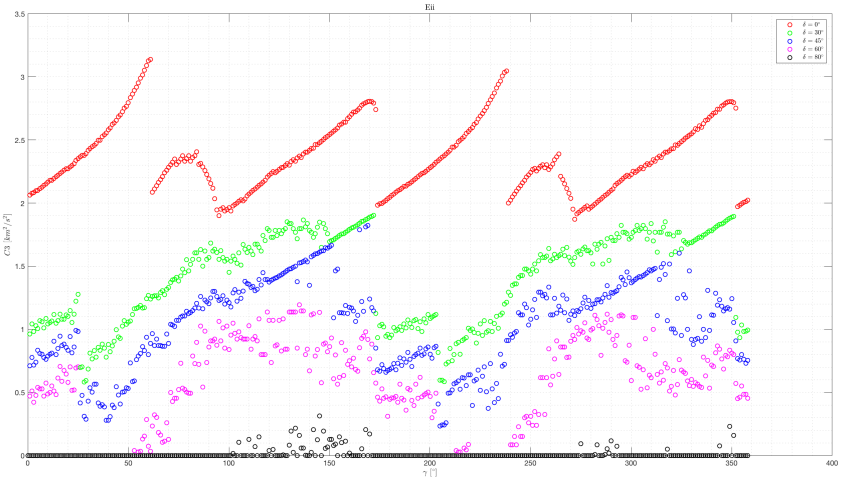

Figure 4.36: $C3_{max}$ function of the flight-path angle (γ) for fixed values of declination (δ) and $V_\infty = 0.9$ Km/s, *Eii* family.

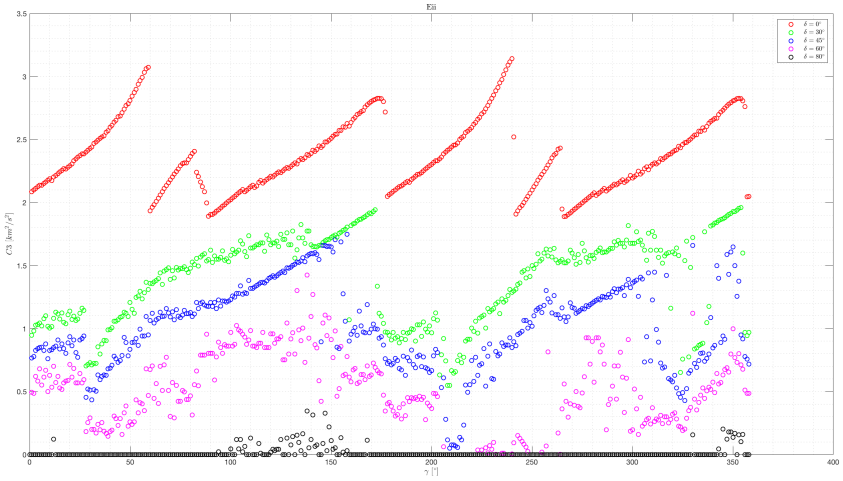

Figure 4.37: $C3_{max}$ function of the flight-path angle (γ) for fixed values of declination (δ) and $V_\infty = 1$ Km/s, *Eii* family.

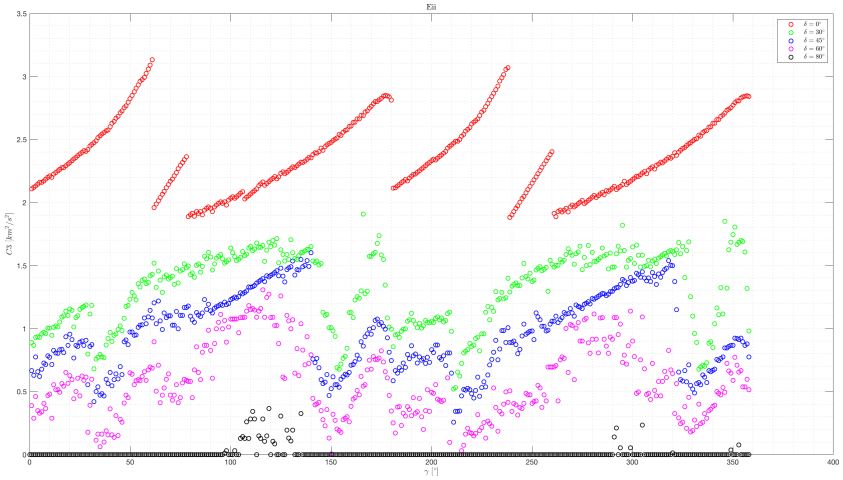

Figure 4.38: $C3_{max}$ function of the flight-path angle (γ) for fixed values of declination (δ) and $V_\infty = 1.1$ Km/s, *Eii* family.

$Foi - Fii$

The irregularities that were evident for D and E families are here even more so. Although there are numerous discontinuities, the trend for the different curves are still perceivable, and it can be noted, ignoring the most important falls, how the minimum $C3$ is grown up when compared to the first families, meaning that escapes that use a 6-month long moon-to-moon leg are more energetic than quicker ones.

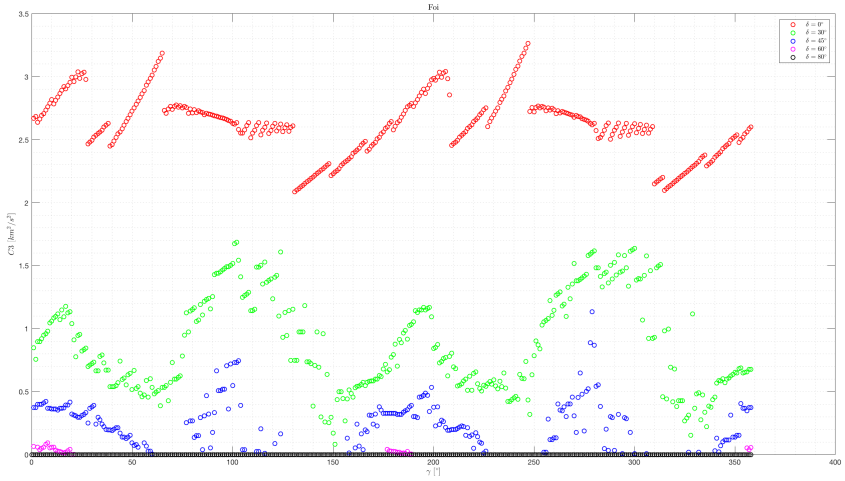

Figure 4.39: $C3_{max}$ function of the flight-path angle (γ) for fixed values of declination (δ) and $V_\infty = 0.9$ Km/s, *Foi* family.

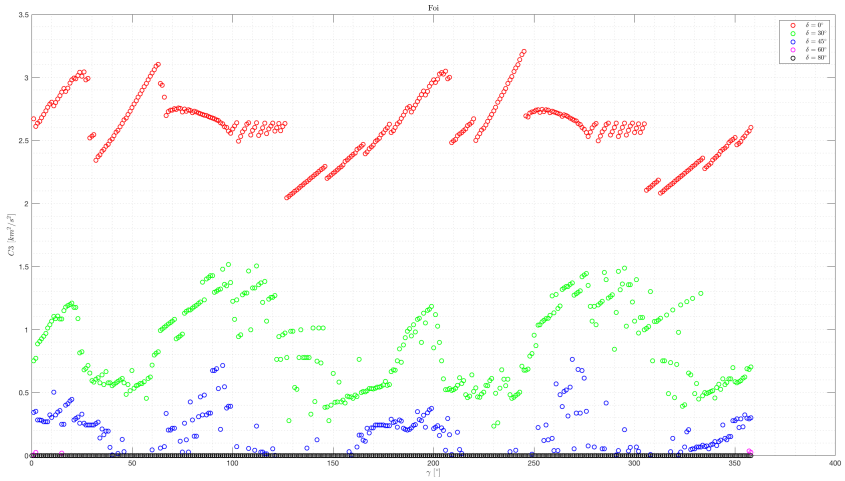

Figure 4.40: $C3_{max}$ function of the flight-path angle (γ) for fixed values of declination (δ) and $V_\infty = 1$ Km/s, *Foi* family.

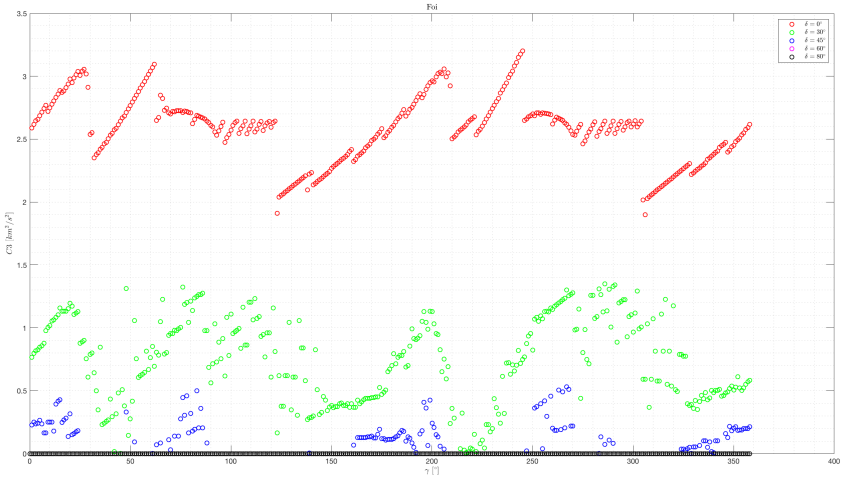

Figure 4.41: $C3_{max}$ function of the flight-path angle (γ) for fixed values of declination (δ) and $V_\infty = 1.1$ Km/s, *Foi* family.

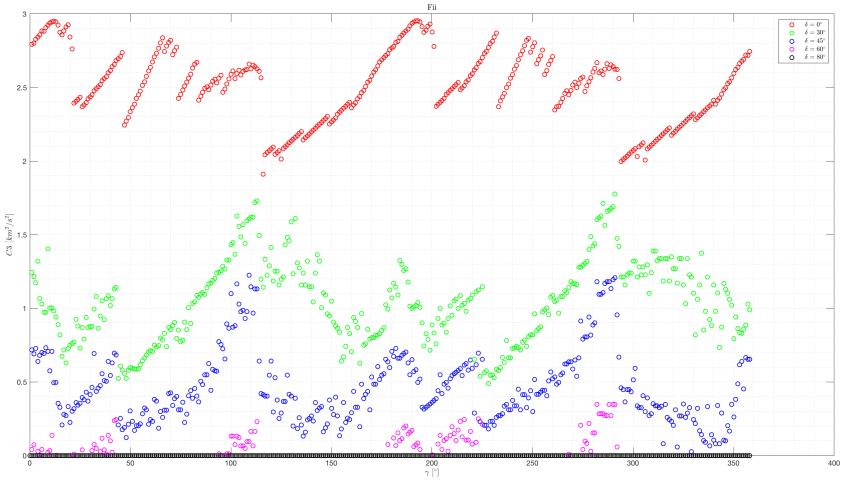

Figure 4.42: $C3_{max}$ function of the flight-path angle (γ) for fixed values of declination (δ) and $V_\infty = 0.9$ Km/s, *Fii* family.

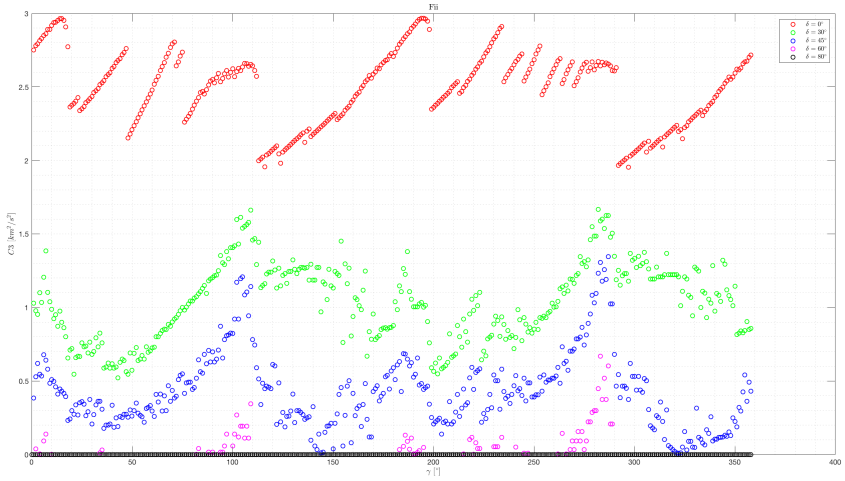

Figure 4.43: $C3_{max}$ function of the flight-path angle (γ) for fixed values of declination (δ) and $V_\infty = 1$ Km/s, Fii family.

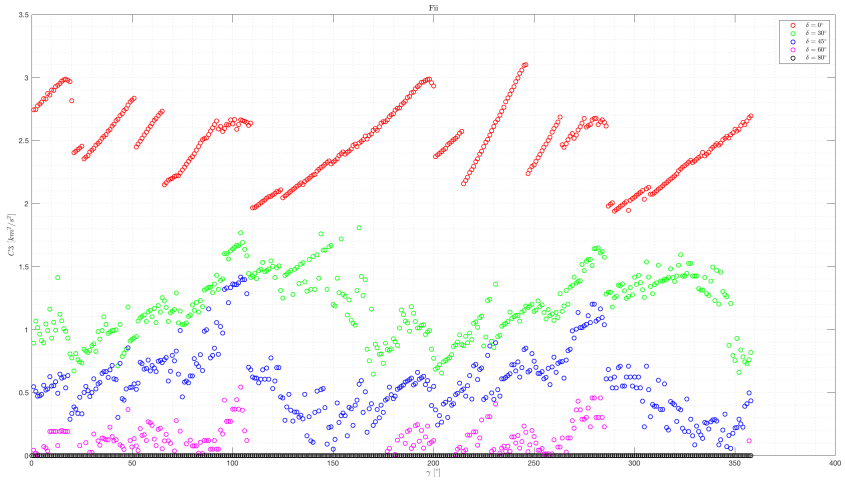

Figure 4.44: $C3_{max}$ function of the flight-path angle (γ) for fixed values of declination (δ) and $V_\infty = 1.1$ Km/s, Fii family.

4.2.2 Global results

Assembling the matrices of every family has been obtained final matrix, as indicated in section 3.2.2. It allows evaluating the global obtainable effect of the lunar gravity assist, regardless of the duration of the moon-to-moon leg employed to sort the different families.

Equally to what has been done for every family, this matrix has been graphically represented using the same colour scale and the trend of $C3(\gamma)$ for the same given values of δ has been plotted.

Two main peaks can be identified: the first, smaller, one is located in the proximity of flight-path angle $\gamma = 30°$, and it achieves $C3 = 3.04\ km^2/s^2$ for a declination of $\delta = 0°$ and each V_∞– equivalent to the first peak of the Foi family, visible in figures from 4.39 to 4.41 ; the second one, on the other hand, is higher and achieves $C3 = 3.21\ km^2/s^2$ for $\gamma \simeq 70°$ and each V_∞– equivalent to the first peak of the Eoi family or the second one for the Foi one.

As concern the minimum value, any combination of flight-path angle and declination gives $C3 \geq 0.5\ km^2/s^2$.

Finally, six additional graphs have been made (figures from 4.48 to 4.53), showing, varying δ and V_∞, the minimum and maximum $C3$,V_{esc} and the ratio V_{esc}/V_∞ achievable, so as to obtain what the guaranteed attainable escape velocity given the desired escape declination and the spacecraft initial velocity relative to Moon is.
For $V_\infty = 1$ Km/s, notwithstanding there are some irregularities, deriving by the ones present in the single families, the trend of the minimum $C3_{max}$ is the following: usually more energetic escapes are had for lower declination, since a smaller part of the gained ΔV is spent for the rotation of the $\boldsymbol{V}$ vector away from the ecliptic plane. With a planar escape – $\delta = 0°$ – the minimum guaranteed escape velocity, independently from the desired flight-path angle,

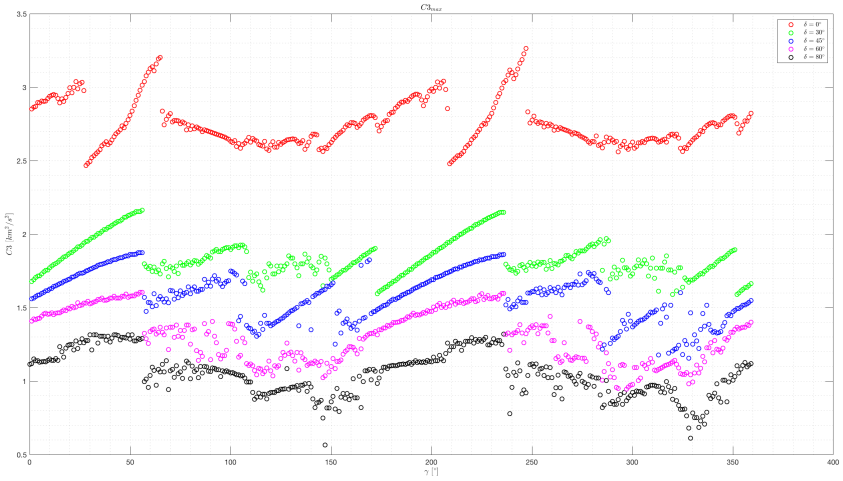

Figure 4.45: $C3_{max}$ function of the flight-path angle (γ) for fixed values of declination (δ) and $V_\infty = 0.9$ Km/s.

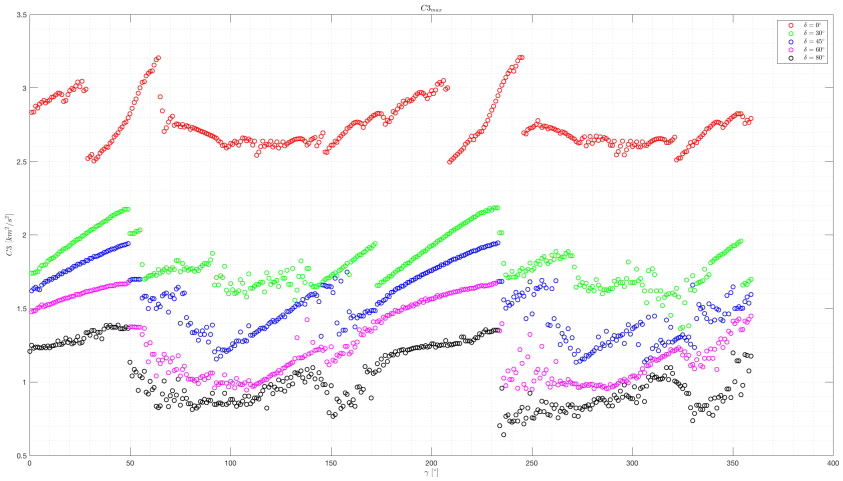

Figure 4.46: $C3_{max}$ function of the flight-path angle (γ) for fixed values of declination (δ) and $V_\infty = 1$ Km/s.

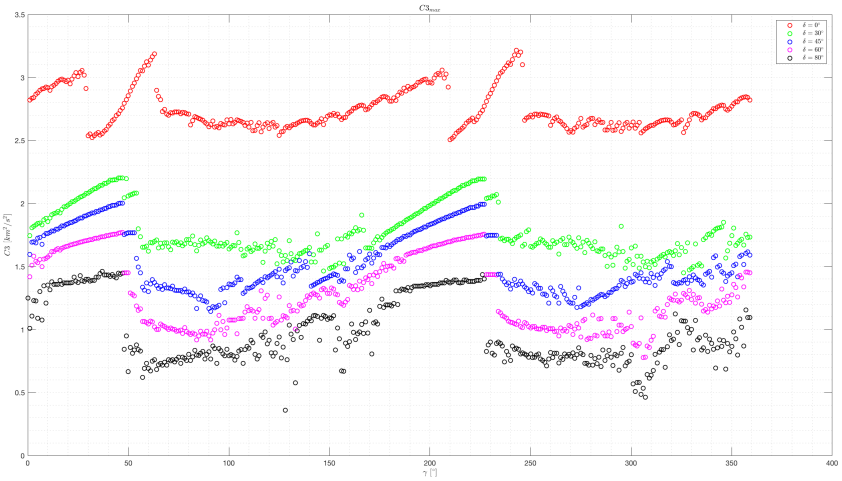

Figure 4.47: $C3_{max}$ function of the flight-path angle (γ) for fixed values of declination (δ) and $V_\infty = 1.1$ Km/s.

is $V_{esc} = 1.57\ km/s$, as the associated $C3$ is 2.5 km^2/s^2. This value remains enough steady until $\delta = 2°$, where it starts to have quickly downhill, shifting to $C3 \simeq 1.58\ km^2/s^2$ and $V_{esc} = 1.26\ km/s$ for $\delta = 26°$; after, are had a more gradual decrease and, for $\delta = 80°$, $C3 \simeq 0.78\ km^2/s^2$ and $V_{esc} = 0.85\ km/s$ is get. Afterwards, it decreases again rapidly until it reaches a $C3 = 0\ km^2/s^2$ for $\delta = 89°$ and consequently also the V is null. The trend of the curves for $V_\infty = 0.9$ Km/s and $V_\infty = 1.1$ Km/s is the same as that just considered, even if the many irregularities present do not allow us to understand the correct effect of the V_∞ on the C3.

Figure 4.51 shows a similar trend for the maximum values for $C3$: starting from $C3 = 3.21\ km^2/s^2$ and $V_{esc} = 1.79\ km/s$, it is had a rapidly decrease until $\delta = 16°$, where the descent becomes more slight, even though with few irregularities, goes on steadily up to $C3 \simeq 1\ km^2/s^2$ for $\delta = 90°$. The trend of the curves for $V_\infty = 0.9$ Km/s and $V_\infty = 1.1$ Km/s is the same as that just considered and also the presence of few irregularities allow us to understand the effect of the V_∞ on the C3: up to $\delta = 18°$ the C3 obtainable, for the different velocities are always the same, while for higher δ values, it is shown that as the velocity increases, higher C3 are obtained and accordingly higher

V_{esc}.

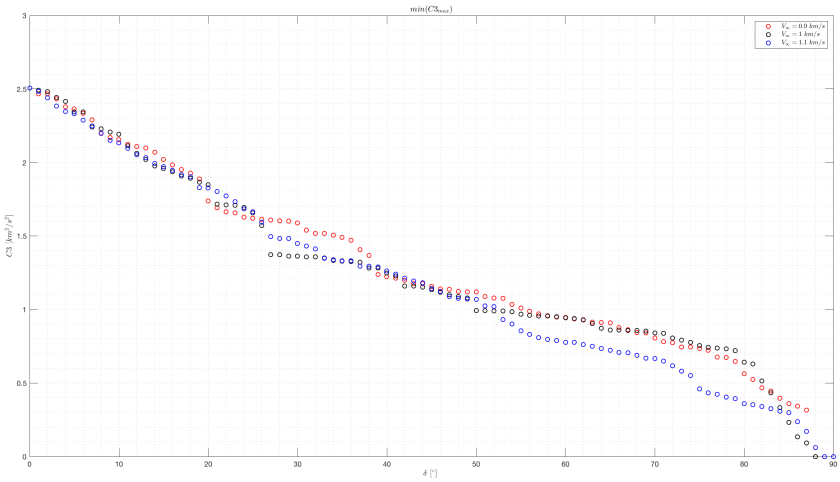

Figure 4.48: Minimum $C3_{max}(\gamma)$ varying with δ and V_∞.

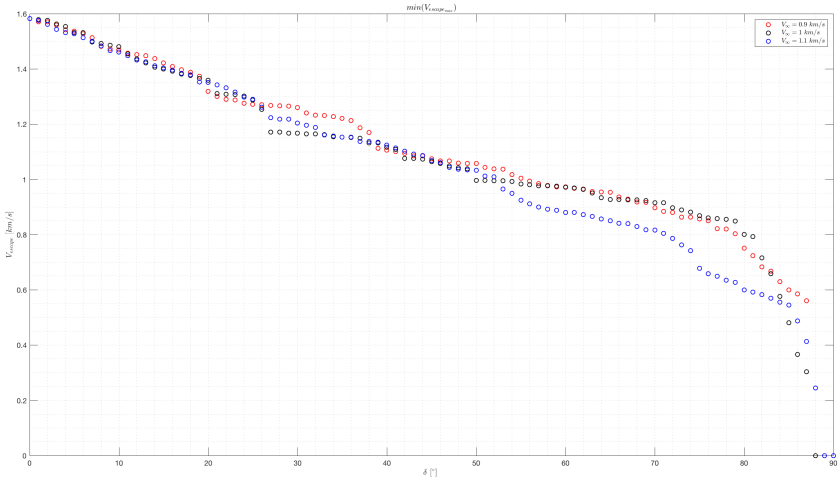

Figure 4.49: Minimum V_{escape} varying with δ and V_∞.

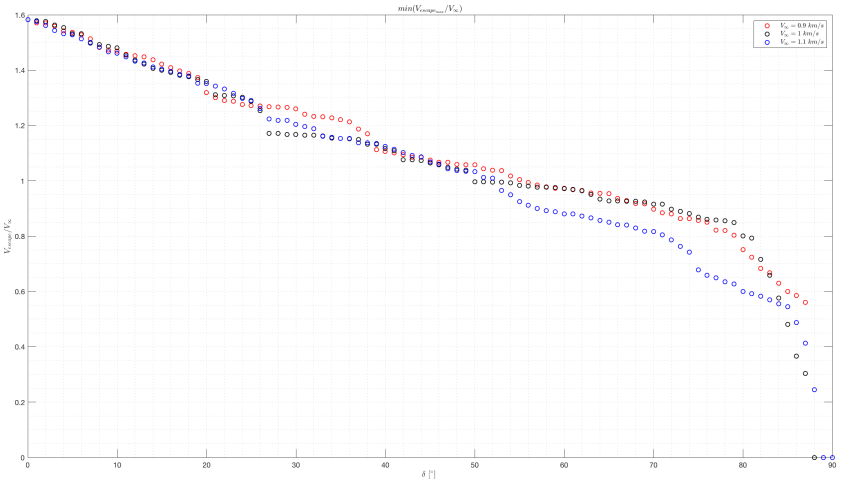

Figure 4.50: Minimum V_{escape}/V_∞ varying with δ and V_∞.

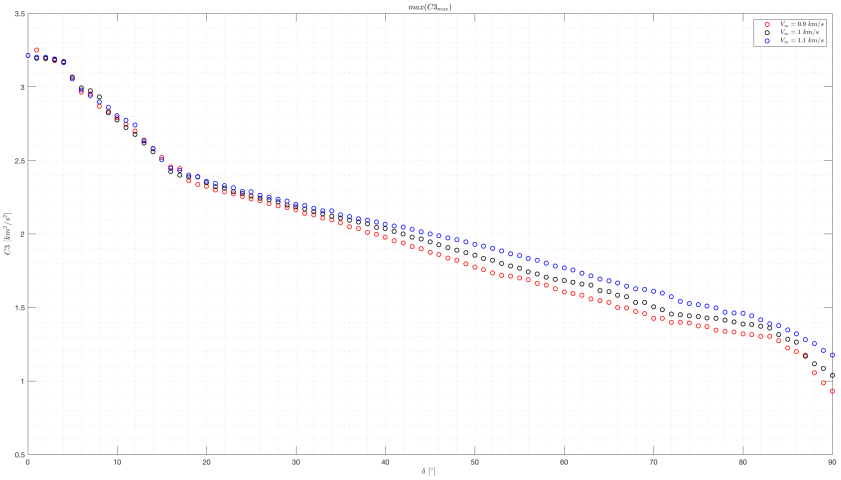

Figure 4.51: Maximum $C3_{max}(\gamma)$ varying with δ and V_∞.

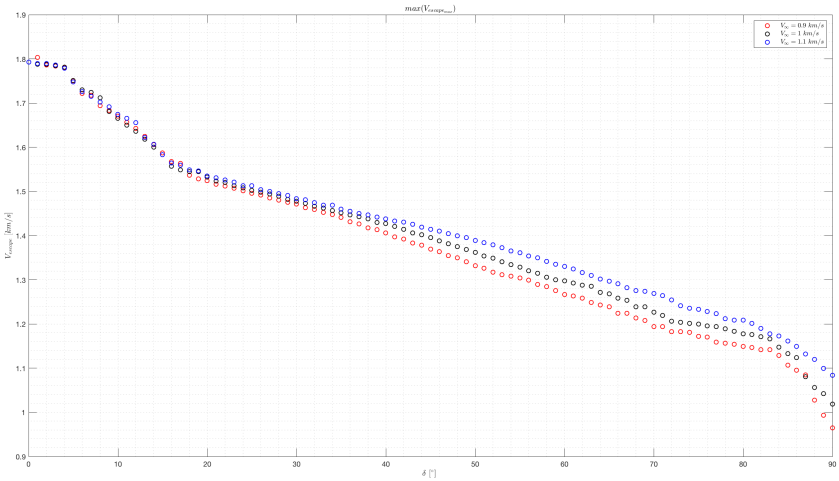

Figure 4.52: Maximum V_{escape} varying with δ and V_∞.

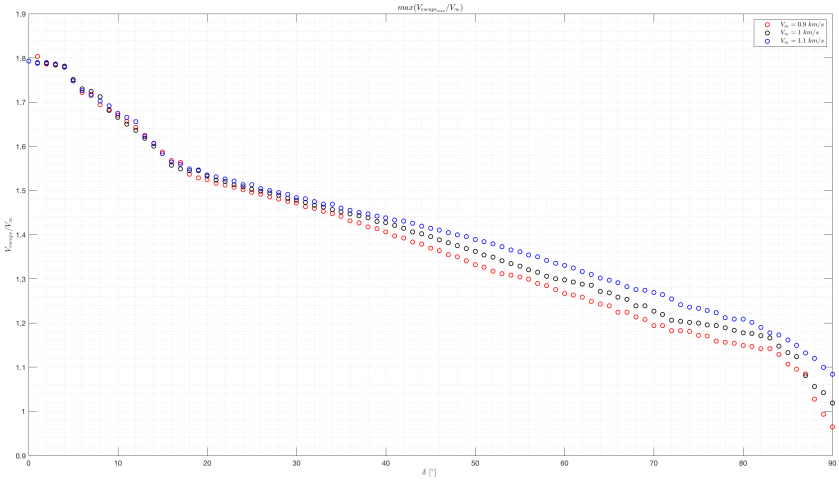

Figure 4.53: Maximum V_{escape}/V_∞ varying with δ and V_∞.

Chapter 5

Conclusions

5.1 Conclusions

The goal of aforesaid work is been to analyze the possibility to carrying out multiple lunar gravity assist escape maneuvers, linking the desired escape conditions (i.e heliocentric flight-path angle and declination) with the obtainable escape velocity, which is the square root of the specific characteristic energy ($C3$). At the beginning, the solar-perturbed orbits that allow two consecutive LGAs have been searched, using the code designed. After, the second LGA has been analyzed for every moon-to-moon transfer identified in the previous step. The obtained data, that correlating heliocentric flight-path angle, declination and the respective $C3$ at the escape to the characteristics of the gravity assist (i.e pump and crank angle) have been interpolated, to straight link a $C3$ to every couple (γ, δ) .Only the case $\delta > 0°$ has been studied since the LGA maneuver is symmetrical.
Observing the obtaining results can be concluded that for interplanetary missions, the lunar gravity assist escape maneuvers allow bringing more payload mass in exchange for longer mission duration, respect to thrust-based escape strategies, since the heliocentric escape velocity attainable is not correlating to used propellant mass. Finally, in a preliminary design phase of an interplanetary mission exploiting lunar gravity assist escape strategy, the previously graphs presented can be used, since they link the characteristics

of the desired heliocentric orbit to the minimum guaranteed escape velocity.

5.2 Future work

The main issue faced during the development of the present study has consisted of elimination of the overlap of the curves for different declination angles and lack of symmetry that occurred in the previous version of the developed algorithm. Although these problems have been solved, the curves are not regular for all families due to the miss of solutions, as discussed in the section 4.2.1; however, it was possible to visualize the general trend of curves. Therefore, the present study might be completed by looking for missing solutions.

Finally, to complete the evaluation of the geocentric part of an interplanetary mission, the present study might be completed by an analysis of the launch and Earth-to-moon phases.

Acknowledgements

I would like to thank prof. Lorenzo Casalino for his availability and for the help given to me in the development and writing of this thesis, with which he allowed me to face practical problems that generally do not meet during the course of studies.

I would like to thank my friends Kevin Masullo and Leonardo Pierro, who during these years, even if far away, have supported me with continuous messages and calls, making the happiest days a few times.

I would also like to thank my girlfriend Rosarita, for making the distance from home less heavy and for being at my side both in positive and negative moments, supporting and encouraging me.

Finally, I must express my gratitude especially to my parents and my sister Samantha, as they have allowed me to achieve this great goal, supporting and giving me good advices during all these years.

Thank you.

Bibliography

[1] Roger R Bate, Donald D Mueller, and Jerry E White. *Fundamentals of astrodynamics*. Courier Corporation, 1971.

[2] Lorenzo Casalino and Lucio Filizola. "Design of High-Energy Escape Trajectories with Lunar Gravity Assist". In: *26th International Symposium on Space Flight Dynamics*. ISTS. 2017.

[3] Lorenzo Casalino and Gregory Lantoine. "Design of Lunar-Gravity-Assisted Escape Maneuvres". In: *2017 AAS/AIAA Astrodynamics Specialist Conference. AAS/AIAA*. Aug. 22, 2017.

[4] Wang Sang Koon et al. "Low energy transfer to the Moon". In: *Dynamics of Natural and Artificial Celestial Bodies*. Springer, 2001, pp. 63–73.

[5] Gregory Lantoine and Timothy P McElrath. "Families of Solar-perturbed moon-to-moon transfers". In: *24th AAS/AIAA Spaceflight Mechanics Meeting. AAS/AIAA*. 2014.

[6] Timothy P McElrath et al. "Using gravity assists in the Earth-Moon system as a gateway to the solar system". In: *Global Space Exploration Conference (GLEX) 2012* (2012).

[7] Melissa L. McGuire et al. "Overview of the mission design reference trajectory for Nasa's Asteroid Redirect Robotic Missions". In: *2017 AAS/AIAA Astrodynamics Specialist Conference. AAS/AIAA*. Aug. 22, 2017.

[8] Isaac Newton. *The Principia: mathematical principles of natural philosophy*. Univ of California Press, 1999.

[9] Hanspeter Schaub and John L Junkins. *Analytical mechanics of space systems*. Aiaa, 2003.

[10] Maurizio Valesani. "Escape trajectories exploiting multiple Lunar gravity assists". Master thesis. Politecnico di Torino, 2018.

[11] David R Williams. *Moon Fact Sheet*. Ed. by NASA. July 3, 2017. URL: `https://nssdc.gsfc.nasa.gov/planetary/factsheet/moonfact.html`.